Heliyon 10 (2024) e30968

Contents lists available at ScienceDirect

Heliyon

journal homepage: www.cell.com/heliyon

Research article

Enhancement of the function of mesenchymal stem cells by using a GMP-grade three-dimensional hypoxic large-scale production system

Yiyao Qi [a,b,1], Xicheng Wang [a,b,1], Zhihui Bai [a,b,1], Ying Xu [a,b], Tingting Lu [a,b], Hanyu Zhu [a,b], Shoumei Zhang [a,b], Zhihong Wu [c], Zhongmin Liu [a,b,**], Zhiying He [a,b,***], Wenwen Jia [a,b,*]

[a] Institute for Regenerative Medicine, School of Life Sciences and Technology, School of Medicine, Tongji University, Shanghai, 200123, China
[b] National Stem Cell Translational Resource Center, Shanghai East Hospital, Tongji University, Shanghai, 200123, China
[c] School of Materials Science and Engineering, University of Shanghai for Science and Technology, Shanghai, 200093, China

A B S T R A C T

Background: Efficiently increasing the production of clinical-grade mesenchymal stem cells (MSCs) is crucial for clinical applications. Challenges with the current planar culture methods include scalability issues, labour intensity, concerns related to cell senescence, and heterogeneous responses. This study aimed to establish a large-scale production system for MSC generation. In addition, a comparative analysis of the biological differences between MSCs cultured under various conditions was conducted.

Methods and materials: We developed a GMP-grade three-dimensional hypoxic large-scale production (TDHLSP) system for MSCs using self-fabricated glass microcarriers and a multifunctional bioreactor. Different parameters, including cell viability, cell diameter, immunophenotype, morphology, karyotype, and tumourigenicity were assessed in MSCs cultured using different methods. Single-cell RNA sequencing (scRNA-seq) revealed pathways and genes associated with the enhanced functionality of MSCs cultured in three dimensions under hypoxic conditions (3D_Hypo MSCs). Moreover, CD142 knockdown in 3D_Hypo MSCs confirmed its *in vitro* functions.

Results: Inoculating 2×10^8 MSCs into a 2.6 L bioreactor in the TDHLSP system resulted in a final scale of 4.6×10^9 3D_Hypo MSCs by day 10. The 3D_Hypo MSCs retained characteristics of the 2D MSCs, demonstrating their genomic stability and non-tumourigenicity. Interestingly, the subpopulations of 3D_Hypo MSCs exhibited a more uniform distribution and a closer relationship than those of 2D MSCs. The heterogeneity of MSCs was strongly correlated with 'cell cycle' and 'stroma/mesenchyme', with 3D_Hypo MSCs expressing higher levels of activated stroma genes. Compared to 2D MSCs, 3D_Hypo MSCs demonstrated enhanced capabilities in blood vessel formation, TGF-β1 secretion, and inhibition of BV2 proliferation, with maintenance of Senescence-Associated β-Galactosidase (SA-β-gal) negativity. However, the enhanced functions of 3D_Hypo MSCs decreased upon the downregulation of CD142 expression.

Conclusion: The TDHLSP system led to a high overall production of MSCs and promoted uniform distribution of MSC clusters. This cultivation method also enhanced key cellular properties, such as angiogenesis, immunosuppression, and anti-aging. These functionally improved and uniform MSC subpopulations provide a solid basis for the clinical application of stem cell therapies.

* Corresponding author.
** Corresponding author.
*** Corresponding author. Institute for Regenerative Medicine, School of Life Sciences and Technology, School of Medicine, Tongji University, Shanghai 200123, China.
E-mail addresses: liu.zhongmin@tongji.edu.cn (Z. Liu), zyhe@tongji.edu.cn (Z. He), wuj3@tongji.edu.cn (W. Jia).
[1] These authors have contributed equally to this work.

https://doi.org/10.1016/j.heliyon.2024.e30968
Received 14 January 2024; Received in revised form 7 May 2024; Accepted 8 May 2024
Available online 18 May 2024

1. Introduction

MSCs are multipotent and possess the unique abilities of self-renewal and differentiation into adipocytes, chondrocytes, and osteoblasts. MSCs can be obtained from various sources, including the bone marrow [1], umbilical cord [2], adipose tissue [3], and umbilical cord blood [4]. MSCs have been recognised to play a crucial role in the body's daily physiological activities and pathological responses, contributing to tissue homeostasis, aging, immune regulation, and tissue repair and regeneration [5-7]. The therapeutic applications of MSCs encompass a wide range of diseases, including orthopaedic diseases, graft-versus-host disease, diabetes, neurological disorders, and heart diseases, with such therapy confirmed to exhibit significant clinical efficacy [8,9]. Notably, MSCs derived from umbilical cords exhibit low immune evasion, making them more suitable for clinical applications and biopharmaceutical Research & Development (R&D) [6,10]. Based on their recognised benefits, the increasing focus on stem cell clinical research and drug development poses a significant challenge to the production of large-yield cells. The traditional two-dimensional (2D) monolayer culture methods used for cell expansion during MSC production are associated with several disadvantages, including limitations in the expansion area, an open culture system that increases the risk of contamination, high dependence on manual labour, lack of real-time monitoring, and difficulty in achieving consistent cell quality from batch to batch. Further, as MSCs are passaged, they enter an aging state with reduced therapeutic efficiency [11]. These limitations may hinder the clinical translation of MSCs [12,13]. Therefore, the development of large-scale MSC expansion technologies is urgently needed.

According to previous studies, the use of a bioreactor for MSC expansion enables a high expansion rate as microcarriers are introduced in a three-dimensional (3D) environment, providing a surface area for cell adhesion and adjustment of the oxygen concentration [14,15]. In the same batch, 3D-hypoxic scale expansion consistently produced significantly higher number of cells with consistent quality than 2D conditions [15]. Bioreactor culture systems have several advantages, including shorter expansion times, full closure, automation of the entire process, reduced dependence on cleanroom space, and lower production costs [14]. Bioreactors are also equipped for online monitoring of crucial culture parameters, such as mass transfer, dissolved oxygen, cell density, pH, temperature, and metabolites [16,17].

The yield of MSCs produced by bioreactors can meet the growing needs of clinical research; therefore, quality control of harvested 3D-cultured MSCs must be carefully considered [10,18,19]. Given the significant differences in conditions between 2D and 3D culture methods, a more thorough exploration of the features and functions of 3D_Hypo MSCs is necessary. Several studies have reported differences in surface markers, proliferative activity, and differentiation functions of MSCs under 3D and hypoxic culture conditions [20-22]. However, a systematic analysis of single-cell gene expression and cell subpopulations is lacking.

In this study, a large-scale, automated, and fully enclosed stirred multifunctional microbioreactor was developed in collaboration with Nanjing Birui Biotechnology Co. Ltd. This bioreactor-microcarrier system was used to establish a good manufacturing Practice (GMP)-grade three-dimensional hypoxic large-scale production (TDHLSP) system for MSC production. This system incorporates four levels of cell banks and a comprehensive quality control chain. MSCs cultured in 3D and under hypoxic conditions (3D_Hypo MSCs) were identified based on their critical quality attributes (CQA) [23]. Single-cell RNA sequencing (scRNA-seq) was performed to generate the single-cell transcriptome profiles of both 2D and 3D MSCs. Enrichment analysis of scRNA-seq and bulk RNA-seq data revealed differences in gene expression between 2D and 3D MSCs. Subsequently, trajectory and non-negative matrix factorization (NMF) analyses were conducted to determine the differentiation trajectories and heterogeneity of MSCs under different culture conditions.

The TDHLSP system addresses the requirements for cell number, standardised quality, and quality benchmarks in both pharmaceutical and clinical studies involving MSCs. Simultaneously, the analysis of scRNA-seq data enhanced our understanding of the molecular mechanisms underlying 3D MSCs. These endeavours lay a theoretical foundation for the translation of MSC therapy from laboratory to clinic.

2. MSCs isolation and culture

Human umbilical cord tissues were obtained from three healthy pregnant donors (patient numbers: 467288, 475610, and 475452) who provided informed consent at Shanghai East Hospital. These donors had negative blood pathogen reports for HIV, HBV, HCV, syphilis, and COVID-19. Wharton's jelly was separated from the umbilical cord by removing the vein and artery, and cut into 1–3 mm^3 pieces. The tissue blocks were placed in T75 cell culture flasks (Corning) and incubated at 37 °C with 5 % CO_2. After 4–6 h of culture, alpha minimal essential medium (α-MEM; Gibco) with 10 % UltraGRO™-Advanced (Helios) was added. Culture was allowed to proceed until the primary MSCs migrated. Thereafter, the medium and tissue slides were discarded. In this process, primary MSCs were isolated from the umbilical cord and cultivated at P1. The resulting P1 cells were frozen in liquid nitrogen to generate P1 seed cells. Thawed cells from the P1 seed cell bank were subcultured to P3, frozen, and stored in the P3 seed cell bank. All procedures were reviewed and approved by the Ethics Committee of Shanghai East Hospital. All production procedures and materials were performed in an International Organization for Standardization 9001:2015-certified Good Manufacturing Practice (GMP) Laboratory under GMP conditions.

3. Process of the TDHLSP system for MSCs

The glass microbeads (1.2 kg) were washed with ultrapure water and immersed in an aqueous NaOH solution for 24 h. The microcarriers were scrubbed 3–4 times using ultrapure water, placed in a reactor tank and soaked in ultrapure water overnight for further use. P3 MSCs were thawed and seeded at a density of 10,000 cells/cm^2 (effective surface area of the 2.6 L reactor: 20,000 cm^2).

Complete serum-free medium for human Mesenchymal Stem Cells (Tianjin Haoyang Biological Manufacture Co., Ltd.) was added. The MSC-microbead mixture was cultured in a 2.6 L bioreactor, and the stirring speed was gradually increased from 1500 rpm to 2500 rpm and then to 3500 rpm under manual control, and adjusted to the automatic control mode after liquid circulation. All cells in the TDHLSP platform were cultured in 5 % oxygen at 37 °C. The harvested 3D and hypoxic MSCs were named 3D_Hypo MSCs. A total of 2×10^8 MSCs at P3, mixed with microbeads, were introduced into a 2.6 L bioreactor and allowed to expand for 5 days. Subsequently, 2×10^9 3DHypo MSCs were harvested and stored in a Master Cell Bank (MCB). A total of 2×10^8 3D_Hypo MSCs from the MCB were continuously cultivated in the bioreactor for an additional five days. Finally, 2×10^9 3D_Hypo MSCs were harvested and designated as the Work Cell Bank (WCB). Thawed P3 MSCs were seeded (10,000 cells/cm^2) in T175 culture flasks (Corning) at 5 % or 20 % oxygen, and the harvested cells were called 2D_Hypo MSCs and 2D_Norm MSCs, respectively.

4. scRNA-seq library preparation and sequencing

Single-cell suspensions (2×10^5 cells/mL) in DPBS (Gibco) were loaded onto a microwell chip using the Singleron Matrix® Single Cell Processing system. Subsequently, Barcoding Beads were collected from the microwell chip, followed by the reverse transcription of mRNA to obtain cDNA. The amplified cDNA of single cells was fragmented and ligated with sequencing adapters. scRNA-seq libraries were constructed based on the GEXSCOPE® Single Cell RNA Library Kits protocol (Singleron) [24]. Individual libraries were diluted to 4 nM, pooled, and sequenced on an Illumina NovaSeq 6000 with 150 bp paired-end reads. The CeleScope software and internal pipeline were leveraged to process the scRNA-seq raw data (available at https://github.com/singleron-RD/CeleScope), and raw reads were processed to generate gene expression profiles. In brief, cell barcodes and UMIs were extracted after filtering read one without poly T tails. Adapters and poly A tails were trimmed (fastp V1) before aligning read two to GRCh38 with Ensemble version 92 gene annotation (fastp 2.5.3a and featureCounts 1.6.2) [25]. The UMI count tables of each cellular barcode were employed for further analysis.

5. Identification of potential cell clusters of MSCs

The downstream analysis of single-cell RNA-sequencing data of MSCs was conducted using the Seurat package (http://satijalab.org/seurat/, v.3.0.1). The normalization function in the Seurat package was employed to normalize scRNA-seq data (normalization method = "LogNormalize" and scale.factor = 10000). Subsequently, the FindVariableFeatures function was utilized to identify highly variable genes (parameters: selection.method = "vst", nfeatures = 3000). Principal component analysis (PCA) was performed based on the significantly variable genes, followed by uniform manifold approximation and projection (UMAP) for visualization using the top 50 principal components. To integrate different MSC samples and mitigate batch effects arising from different sample collection time points, the CCA integration tool was applied. The FindIntegrationAnchors function was used to identify integration anchors, followed by data integration using the IntegrateData function. The FindAllMarker function was employed to identify differentially expressed genes (DEGs). Furthermore, the Cor function was used for correlation analysis between subpopulations and samples, and radar plots were utilized to display these correlations.

6. Enrichment analysis of MSCs cultured in different conditions

Functional enrichment analysis of marker genes for each subpopulation or group was carried out using the Metascape website (http://www.metascape.org), with results visualised using the R package [26]. Additionally, enrichment analysis of hallmarks for single-cell subpopulations was performed using the irGSEA package (https://github.com/chuiqin/irGSEA/). Gene sets with p-values less than 0.05 were considered statistically significant.

7. Trajectory analysis of the subpopulations of MSCs

Three methods were employed for pseudotime trajectory analysis. Firstly, a pseudotime trajectory was determined using the default settings of the Monocle2 software package. The DDRTree method was applied for dimensionality reduction with max_components set to 2, and the orderCells function was used to sort the cells. Genes exhibiting dynamic expression along the pseudotime were clustered using the "plot_pseudotime_heatmap" function, and the "plot_genes_branched_heatmap" function was used to visualize gene expression in the branching modules. Secondly, RNA velocity, based on actual transcription dynamics, was utilized to study the dynamic differentiation of cellular gene expression. It can predict the differentiation direction and relationships between different subgroups of MSCs without prior knowledge of the developmental process. In this study, the velocyto.R package was used for visualizing RNA velocity through RNA-seq plotting (devtoolsinstall_github ("velocyto-team/velocyto.R″). Thirdly, SCORPIUS infers the linear developmental trajectory of cells using scRNA sequencing data (https://github.com/rcannood/SCORPIUS). With the SCORPIUS package, we performed dimensionality reduction and clustering on single-cell sequencing data of MSCs. The developmental trajectory of cells along the pseudotime under different conditions was based on the cell pseudotime. In this study, SCORPIUS analysis was employed to further confirm the differential levels of heterogeneity and differentiation trajectories of MSCs under different culture conditions, especially the patterns of cell distribution.

8. NMF analysis

NMF is a commonly used clustering algorithm applied for subpopulation analysis. NMF analysis was conducted separately for each MSCs sample to generate programs capturing heterogeneity within each sample. Given the requirement of an influential parameter "K" in NMF application, we ran NMF with different values (K = 4, 5, 6, 7, 8, and 9) to generate diverse numbers of programs with potential biological significance for each MSCs sequencing sample. Each NMF program summarized the top 50 genes based on NMF coefficients. We identified the most significant NMF programs as those universally present across different values of K and different MSCs samples [27]. Subsequently, correlation analysis was performed on all programs based on the clustering results to obtain a more central set of programs. The cNMF analysis was conducted using Python (https://github.com/dylkot/cNMF/), and the enrichment analysis of the programs was performed on the web server (https://metascape.org/gp).

9. Bulk RNA-seq for MSCs

Raw data (in fastq format) were initially processed through in-house perl scripts. In this step, clean data (clean reads) were obtained by removing reads containing adapters, reads with poly-N sequences, and low-quality reads from the raw data. All downstream analyses were conducted using clean data of high quality. Adaptor sequences and low-quality reads were eliminated during this data processing step. The raw sequences were transformed into clean reads, which were then mapped to the reference genome sequence. Only reads with a perfect match or one mismatch were further analysed and annotated based on the reference genome. Hisat2 tools were employed for mapping with the reference genome (Beijing Tsingke Biotech Co., Ltd).

10. Quantitative real-time polymerase chain reaction (qRT-PCR)

Total RNA was extracted from the MSCs of three groups using TRIzol reagent (Ambion). An equal amount of total RNA was subjected to reverse transcription using the PrimeScript™ RT reagent Kit with gDNA Eraser (Tiangen Biotech, Beijing), according to the manufacturer's instructions. qRT-PCR was performed on a 7500 Fast Dx Real-Time PCR Instrument (Applied Biosystems) using SYBR Premix Ex Taq with ROX (Takara RR820A), and the data were analysed using the 7500 Fast System software (v1.5.1). The amplification results were normalised to the GAPDH mRNA levels in each sample. The primers used for gene expression detection are listed in Table 1.

11. Western blot

Proteins were obtained from cellular lysates incubated with RIPA buffer supplemented with a Protease Inhibitor Cocktail (100:1 V/V%, MedChemExpress) and PMSF (100:1 V/V%, Beyotime). Protein quantification was performed using the Omni-Easy™ Instant BCA Protein Assay Kit (Shanghai Epizyme Biomedical Technology Co., Ltd). Equal amounts of the proteins were loaded onto a 10 % SDS-PAGE gel (PAGE Gel Fast Preparation Kit; Shanghai Epizyme Biomedical Technology Co., Ltd.). The proteins were then transferred onto a PVDF membrane and blocked with 5 % nonfat milk. The membrane was incubated with primary antibodies against CD142 (Tissue factor Monoclonal antibody, Proteintech Group, Inc) and GAPDH (Proteintech Group, Inc) at 4 °C overnight, followed by secondary antibodies (horseradish peroxidase-conjugated Affinipure Goat Anti-Mouse IgG(H + L), Proteintech Group, Inc.) at 25 °C for 1 h. Finally, the PVDF membrane was incubated with the appropriate reagent from the Omni-ECL™ Femto Light Chemiluminescence

Table 1
Primer sequences.

Name	Primer	Sequence
CD142	Forward	GGCGCTTCAGGCACTACAA
	Reverse	TTGATTGACGGGTTTGGGTTC
COL5A1	Forward	GCCCGGATGTCGCTATACAG
	Reverse	AAATGCAGACGCAGGGTACAG
COL1A2	Forward	GGCCCTCAAGGTTTCCAAGG
	Reverse	CACCCTGTGGTCCAACAACTC
COL1A1	Forward	GAGGGCCAAGACGAAGACATC
	Reverse	CAGATCACGTCATCGCACAAC
COL11A1	Forward	ACCCTCGCATTGACCTTCC
	Reverse	TTTGTGCAAAATCCCGTTGTTT
VCAN	Forward	GTAACCCATGCGCTACATAAAGT
	Reverse	GGCAAAGTAGGCATCGTTGAAA
FN1	Forward	CGGTGGCTGTCAGTCAAAG
	Reverse	AAACCTCGGCTTCCTCCATAA
POSTN	Forward	CTCATAGTCGTATCAGGGGTCG
	Reverse	ACACAGTCGTTTTCTGTCCAC
CTHRC1	Forward	CAATGGCATTCCGGGTACAC
	Reverse	GTACACTCCGCAATTTTCCCAA
GAPDH	Forward	CATACCAGGAAATGAGCTTG
	Reverse	ATGACATCAAGAAGGTGGTG

Kit (Shanghai Epizyme Biomedical Technology Co., Ltd.). Images were captured using the ChemiDoc XRS + Gel Imaging system (BIO-RAD) and analysed using Image Lab (6.0.1).

12. Telomeric repeat amplification protocol (TRAP) assay

Human skin fibroblasts (HSFs, negative control), human induced pluripotent stem cell (iPSC, positive control), or MSCs of 2D and 3D conditions were extracted using CHAPS solution for 30 min on ice, and then centrifuged at 13,000 g for 30 min at 4 °C. The supernatant was transferred into a 1.5 ml RNase-free EP tube. Total protein was quantified using an Omni-EasyInstant BCA Protein Assay Kit (Shanghai Epizyme Biomedical Technology Co., Ltd.). The cell extract (3 μ g protein) and TS primers (Shanghai Generay Biotech Co., Ltd) were added to the telomerase extension reaction and incubated for 45 min at 30 °C for PCR amplification. The telomerase extension reaction solution and ACX primers (Shanghai Generay Biotech Co., Ltd., Shanghai, China) were subjected to 34 PCR cycles. The PCR products were electrophoretically separated on a 15 % acrylamide gel. The bands were visualised via staining with a nucleic acid dye (TIANGEN BIOTECH, Beijing). Telomerase activity was analysed using a TGel Image System (TIANGEN BIOTECH, Beijing).

13. Flow cytometric analysis

All MSCs were incubated with specific surface markers (positive markers: CD90, CD73, and CD105; negative markers: CD11b, CD19, CD34, CD45, and HLA-DR, BD Biosciences, Franklin Lakes, NJ, USA) for 30 min at 4 °C in the dark. The cells were washed once with Dulbecco's phosphate-buffered saline (DPBS; Gibco) and suspended in test tubes containing DPBS (Gibco). Subsequently, the cells were observed and analysed using flow cytometry (BD, FACSCanto II) and FACSDiva software (V6.1.3, BD)

14. Collection of the MSC conditioned medium

Three types of MSCs in complete serum-free medium for human Mesenchymal Stem Cells (Tianjin Haoyang Biological Manufacture Co., Ltd.) were seeded in T75 cell culture flasks (Corning) at a density of 7×10^5 cells overnight. The medium was then replaced with basic Serum-Free Medium for Human Mesenchymal Stem Cells (Tianjin Haoyang Biological Manufacture Co., Ltd.) for 72 h. The culture supernatant was collected and centrifuged (4 °C, 2000 rpm) for 10 min to remove the cell debris. The resulting supernatant, referred to as the conditioned medium, was stored at −20 °C for long-term use, with repeated freezing and thawing avoided.

15. Inhibition of BV2 proliferation

The mouse microglial cell line (BV2) was procured from the Shanghai Rongmin Biotechnology Center and verified for the absence of endotoxins, bacteria, and mycoplasma. BV2 cells were seeded in a 96-well plate at a density of 1×10^4 cells per well in 100 μL Dulbecco's Modified Eagle Medium (DMEM, Gibco) supplemented with 10 % foetal bovine serum (FBS; Ausbian) overnight. Subsequently, the cells were incubated with 10 % FBS in DMEM (positive control) or MSC-conditioned medium from different groups for 48 h. After the incubation period, 10 μL of CCK8 was added to each well for 4 h. The optical density (OD) was measured at 450 nm using an EnSight multimode board reader (PerkinElmer). Data were collected and analysed using Kaleido software (version 2.0). The BV2 proliferation inhibition ratio was calculated using the following formula: (1 - OD values of (positive control group/treated group)) × 100 %.

16. Tube formation assay

Matrigel (60 μL/well, Corning) was incubated in a 96-well plate at 37 °C for 30 min. Human umbilical vein endothelial cells (HUVECs) at a density of 3×10^4 cells per well were suspended in the corresponding MSC conditioned medium and then added onto the Matrigel in each well. After 4 h (basal) and 16 h, images were captured using an Olympus Microscope (scale bar: 200 μm). The tube formation ratio was calculated using the following formula: (number of tubes at 16 h/number of tubes at 4 h) × 100.

17. Enzyme-linked immunosorbent assay

The conditioned medium from each group of MSCs was used to determine the level of TGF-β1, according to the instructions of the Human TGF-β1 Valukine ELISA kit (Novus Biologicals). The OD values were measured using an EnSight multi-mode board reader (PerkinElmer) and quantified using Kaleido software (2.0).

18. Trilineage differentiation potency

Chondrogenic Differentiation: A total of 6×10^4 MSCs were resuspended in 20 μL of complete Serum-Free Medium for Human Mesenchymal Stem Cells (Tianjin Haoyang Biological Manufacture Co., Ltd) and seeded in the centre of the wells of a 24-well plate (Thermo Fisher Scientific) for cell cluster formation. After 2 h, 1 mL of StemPro™ Chondrogenesis Differentiation medium (Gibco) was added per well, with medium change every other day to induce chondrocyte production. After 19 days, the cells were fixed with 4 % paraformaldehyde (PFA, Beijing Solarbio Science & Technology Co., Ltd.) and stained with Alcian blue solution (Cyagen Biosciences Inc.).

Adipogenic/Osteogenic Differentiation: Confluent MSCs cultured in 6-well plates (Thermo Fisher Scientific) were treated with 2 mL of MesenCult™ Adipogenic Differentiation medium (STEMCELL) or 2 mL of MesenCult™ Osteogenic Differentiation medium (STEMCELL) every 2 days. After 18 days of culture, the cells were fixed with 4 % PFA and stained with Oil Red O or Alizarin Red (Cyagen Biosciences Inc.) for adipogenic and osteogenic differentiation, respectively.

All images were recorded using an Olympus microscope (CKX41, scale bar: 200 μm).

19. Senescence assay

MSCs from the three different culture conditions were seeded in a six-well plate and then fixed with 4 % PFA. The cellular aging state was assessed using the Senescence-Associated-β-galactosidase (SA-β-gal) staining assay kit (Beyotime) according to the manufacturer's instructions. For analysis, three random optical fields were captured using a microscope (CKX41, Olympus) (scale bar: 200 μm).

20. Karyotype analysis

Karyotype analysis of MSCs from both 2D and 3D cultures was conducted at Shanghai Zhenhe Biotechnology Co., Ltd. using standard protocols for high-resolution G-banding.

21. Tumorigenic assay

Matrigel (Corning) was mixed with 1×10^6 3D_Hypo MSCs, 2D_Hypo MSCs, 2D_Norm MSCs, and HeLa cells (positive control) on ice. The cell mixture was subcutaneously injected into 4-week-old male NOD/SCID mice (Charles River). After a 4-week period, mice were observed and images were captured.

22. Soft agar colony formation assay

Low Melting Point Agarose (0.7 % and 1.2 % (Yeasen Biotechnology (Shanghai) Co., Ltd.) was autoclaved for sterilisation. The agarose (1.2 %) was mixed in a 1:1 ratio with 2 × RPMI 1640 medium (Gibco) containing 20 % FBS (Ausbian). The resulting mixture was added to the bottom layer of a 6-well plate (Thermo Fisher Scientific). A single-cell suspension (comprising 3D_Hypo MSCs, 2D_Hypo MSCs, 2D_Norm MSCs, and HeLa cells) was added to the solution, which was mixed in a 1:1 ratio with 0.7 % agarose and 2 × RPMI 1640 medium (Gibco) supplemented with 20 % FBS (Ausbian). The plates were then incubated at 37 °C with 5 % CO_2 for 4 weeks and images were captured using an Olympus microscope (CKX41, scale bar: 200 μm).

23. In vitro transfection with short hairpin RNA (shRNA)

The primer sequences used were sense GGACUUUAGUCAGAAGGAATT and antisense UUCCUUCUGACUAAAGUCCTT. The shRNA was inserted into the lentiviral vector, pLKO.1. The transfection solution consisted of plasmids (VSVG, PAX2, pLKO.1, or CD142 shRNA; Shanghai Generay Biotech Co., Ltd.), X-tremeGENE HP DNA Transfection Reagent (Roche), and Opti-MEM (Gibco), which were mixed lightly and allowed to stand for 15 min at room temperature. The mixture was then gently added to 293T cells. After 48 h of incubation, the lentiviral supernatant was evenly distributed into freeze-storage tubes and stored at −80 °C for future use. 3D_Hypo MSCs were seeded in a 6-well plate (Thermo Fisher Scientific) for 24 h and then introduced in the lentiviral supernatant and DMEM containing 10 % FBS in a 1:1 (V/V %) ratio, in addition to polybrene (4 μg/mL), for 48 h. The mRNA and protein expression levels were evaluated using qRT-PCR and western blotting, respectively.

24. Statistical analysis

Statistical analyses were conducted using GraphPad Prism software (version 7.0a). Data are expressed as mean ± SEM. The significance of the differences was determined using an unpaired two-tailed Student's t-test. One-way ANOVA followed by the Newman-Keuls Multiple Comparison test was employed for intergroup comparisons. All experiments were performed at least three times. Statistical significance was set at $p < 0.05$. 3.

25. Results

25.1. Processes of the TDHLSP system for expanding MSCs

We established a TDHLSP system for MSC expansion, which comprised real-time monitoring of pH, glucose, and lactic acid levels. MSCs were found to adhere to the glass microspheres to enhance their specific surface area for cell culture. The TDHLSP system created a hypoxic environment in the bioreactor by infusing O_2, N_2, CO_2, and air at a rate of 0.5 L/min. The final O_2 partial pressure was maintained at 5 % to mimic the microenvironment of human tissue. Traditionally, MSCs are cultured *in vitro* under 2D conditions in 20 % oxygen. However, our TDHLSP system more accurately replicated physiological conditions, with MSCs adhering to microcarriers and immersed in a 3D environment with 5 % oxygen partial pressure, simulating the microenvironment of the body. Thereafter, we

established a comprehensive large-scale preparation and quality control process for MSCs (Fig. 1). MSCs from both P1 and P3 seed cell banks were subjected to release testing, including assessments for sterility, cell viability, diameter, and mycoplasma. Subsequently, P3 seed cells were used for the industrial-scale expansion of MSCs using the TDHLSP system. CQA assessments were conducted before storing 3D_Hypo MSCs in the MCB and WCB, including evaluations of human viruses, karyotype, surface markers, trilineage differentiation, immunosuppression, tumourigenicity, sterility, mycoplasma, morphology, cell viability, and diameter. Due to the cryopreservation of 3D_Hypo MSCs using a ready-to-use cryopreservation solution, no post-thaw culture was required. This approach mitigated the impact of 2D conditioned culture on the function of 3D_Hypo MSCs. Consequently, 3D_Hypo MSCs from WCB can be readily employed for clinical research after thawing and passing release testing, including assessments of sterility, mycoplasma, cell viability, and diameter.

25.2. *Characterisation of MSCs expanded using the TDHLSP system*

MSCs from three donors were selected for expansion under 3D and hypoxic conditions in a 2.6 L bioreactor. An average of 2×10^8 MSCs (P3) were initially seeded, which led to 2.4×10^9 3D_Hypo MSCs after 5 days, and a total of 4.6×10^9 3D_Hypo MSCs on day 10 (Fig. 2A). Quality control, including the assessment of human viruses (Table S1), sterility, and mycoplasma, yielded negative results for 3D_Hypo MSCs from the MCB and WCB (Table S2).

An observable difference in the cell diameter of the 3D_Hypo MSCs, which was notably shorter than that of 2D-cultured MSCs, was found (Fig. 2B). However, the viability of MSCs cultured in both the 3D and 2D environments exceeded 90 %, with no significant differences found among the three groups (Fig. 2C). 3D_Hypo MSCs adhered to the plastic and displayed a typical fibroblast-like spindle shape, consistent with that of 2D-cultured MSCs (Fig. 2D) [23,28]. As a hallmark of MSCs, their capacity for trilineage differentiation was assessed. MSCs cultivated in both 2D and 3D modes could differentiate into osteocytes, chondrogenic pellets, and adipocytes based on positive Alizarin Red, Alicin Blue, and Oil Red O staining, respectively (Fig. 2E).

The 3D_Hypo MSCs were also slightly smaller than the 2D MSCs. Karyotype analysis was performed to assess the genomic stability of MSCs in 3D and hypoxic cultures. The analysis revealed the presence of the expected 22 chromosome pairs and two sex chromosomes (46XX and 46XY), indicating the absence of chromosomal abnormalities in the MSCs from all three groups (Fig. 2F).

To characterise the 3D_Hypo MSCs, cell surface markers were quantified using flow cytometry. MSCs from both the 2D and 3D modes exhibited high expression levels (>95 %) of the three positive surface markers, CD73, CD90, and CD105. Importantly, none of the cells expressed (<2 % positive) negative surface markers, such as CD45, CD34, CD14, CD11b, CD79, CD19, and HLA-DR (Fig. 2G and S1). To evaluate tumourigenicity, the soft agar colony formation results illustrated in Fig. 2H confirmed the absence of clones in both 3D and 2D cultured MSCs, in contrast to the positive control HeLa cells. Telomerase activity was evaluated. The telomerase activity of 3D_Hypo MSCs was similar to those of HSF (negative controls) and iPSC (positive controls). Unlike most telomerase-negative somatic cells, adult stem cells typically exhibit low to moderate telomerase activity. Notably, the increased activity within a certain range observed in 3D_MSCs compared with 2D MSCs was associated with an enhanced self-renewal capacity (Fig. 2I). This finding contributes to the characterisation of 3D_Hypo MSCs and supports their potential therapeutic applications [29].

To further confirm the identity and source consistency of 2D_Norm MSCs and 3D_Hypo MSCs, 20 STR loci and 1 sex locus were analysed; however, a complete match was found (Fig. S2). These findings collectively indicate that 3D_Hypo MSCs meet the defined

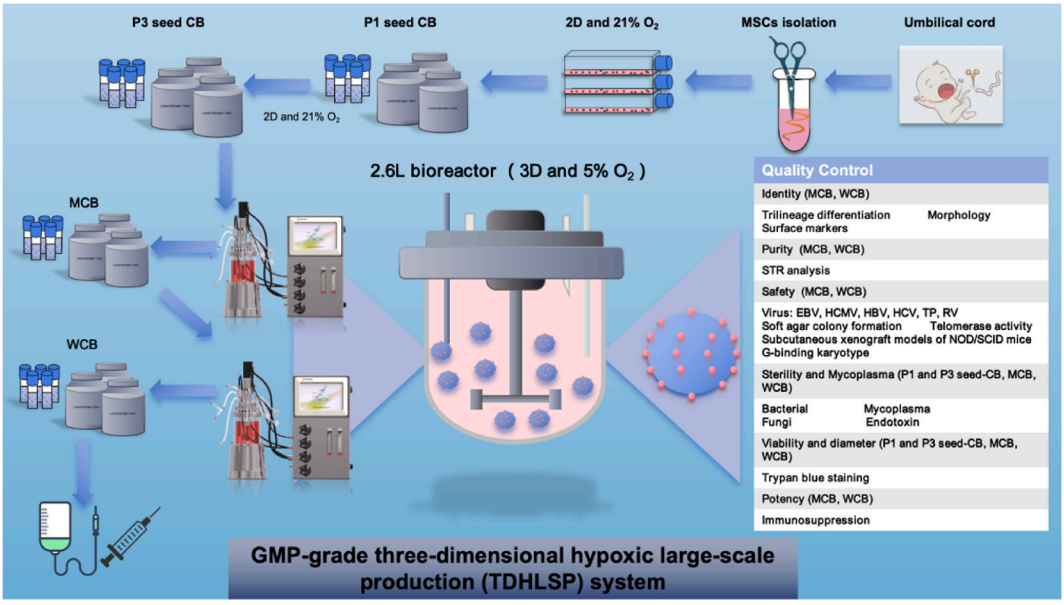

Fig. 1. Processes of the TDHLSP system for expanding MSCs.

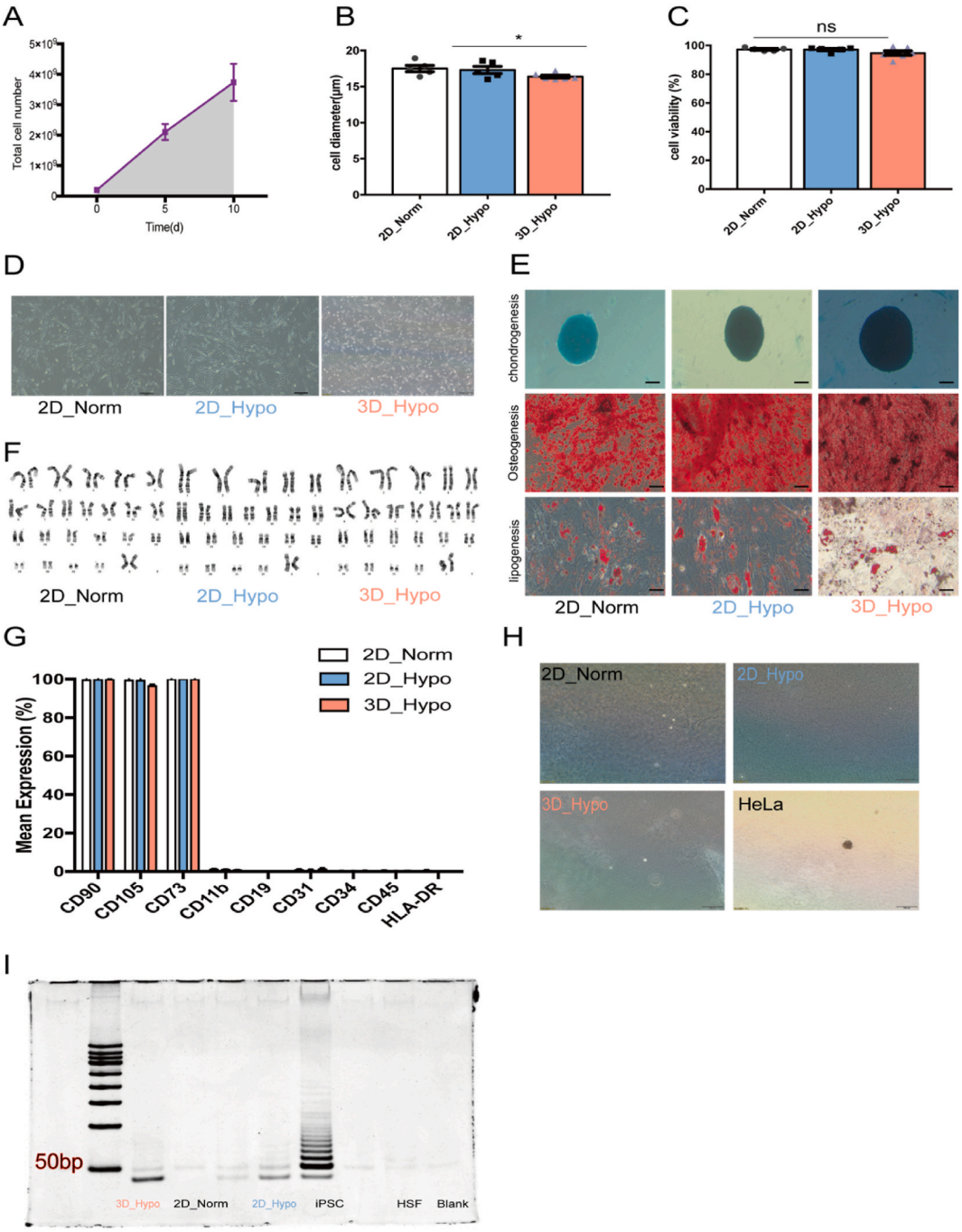

Fig. 2. Characterisation of MSCs expanded using the TDHLSP system. A: Total cell number curve of MSCs cultured using the TDHLSP platform. B–D: Cell diameter (B), cell viability (C), morphology (D), n ≥ 3. Student's t-test. *$p < 0.05$. E: *In vitro* differentiation of 2D and 3D cultured MSCs: osteoblasts, adipocytes, chondrocytes. F: Karyotyping of 2D or 3D expanded MSCs. G: Surface markers (positive markers: CD90, CD105, CD73; negative markers: CD11b, CD19, CD31, CD34, CD45, HLA-DR) expressed in three groups of cultured MSCs. H: Soft agar colony forming ability of 2D and 3D cultured MSCs. I: Telomerase activity of 2D and 3D cultured MSCs. iPSC served as the positive control, HSF served as the negative control, Scale bar: 100 μm.

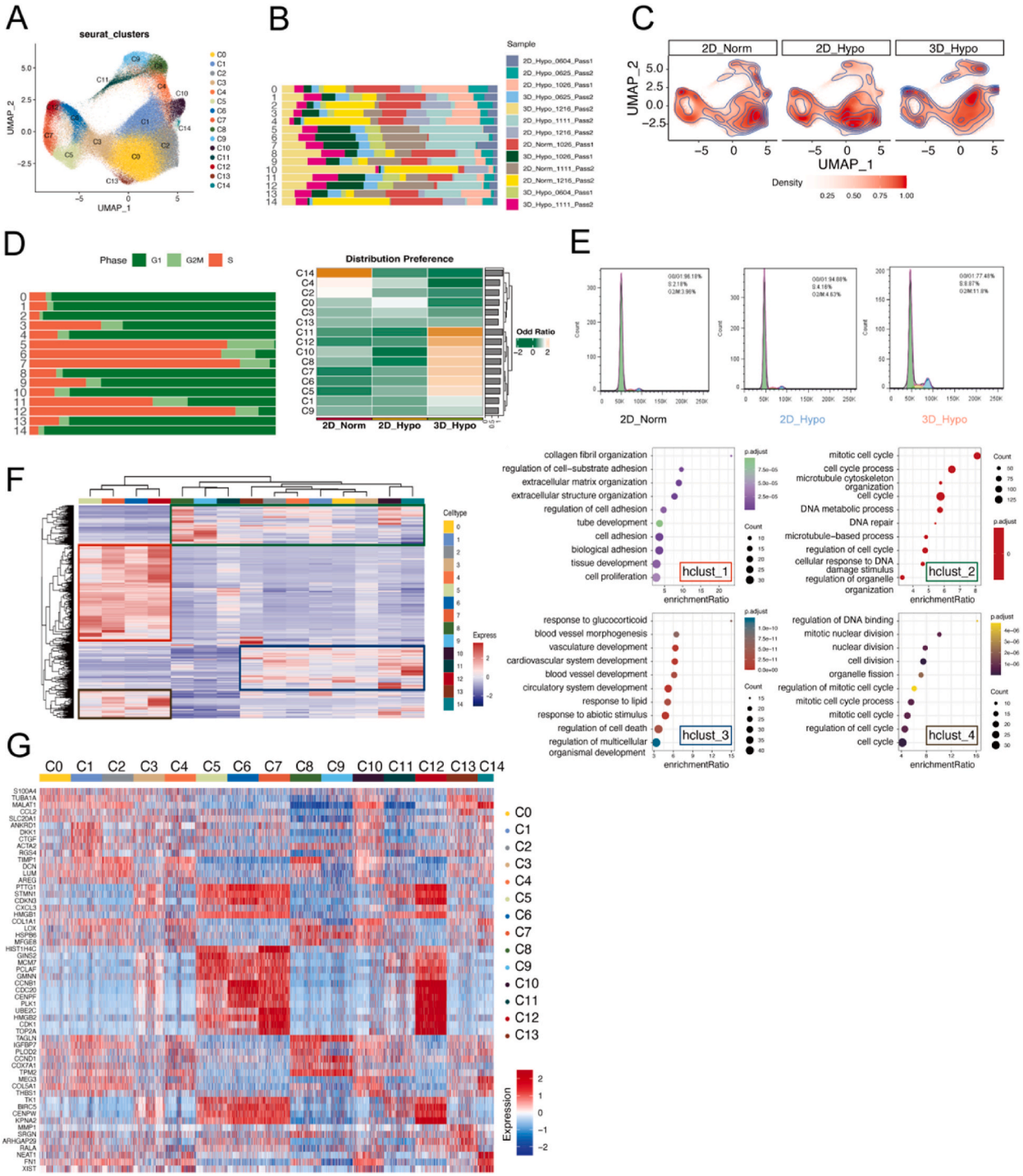

Fig. 3. Single-cell transcriptome atlas of MSCs. A: UMAP visualization of single-cell clusters of MSCs. Cluster analysis of MSCs using the Seurat package. A total of 15 subpopulations were identified in MSCs subjected to three culture conditions. B: Cell proportion of all 15 subpopulations in different samples. C: Cell density of all 15 clusters in the three culture conditions. D: Cell proportion in different cell cycle phases, including the G1, G2M, and S phases. The cell cycle phases were calculated using the Seurat package. Cell distribution preference of all 15 subpopulations in the three culture conditions. Odd ratio value was adopted to estimate the distribution preference. E: Cell cycle detected by Flow Cytometry. F: Enrichment analysis of the top genes, which were classified into four gene clusters. G: Up-regulated genes in 15 clusters.

criteria for MSCs [23,30]. Importantly, the safety profile was emphasised by the non-tumourigenic nature observed in the *in vivo* assays, supporting the potential suitability of these cells for therapeutic applications.

25.3. Single-cell transcriptome atlas of MSCs

After evaluating the general characteristics, we investigated the cellular diversity and transcriptional signatures of MSCs using single-cell transcriptomic analysis. scRNAseq was performed on 2D_Norm MSCs, 2D_Hypo MSCs, and 3D_Hypo MSCs from three donors using the GEXSCOPE® Single Cell RNA Library Kits. The scRNA-seq transcriptomes from these three culture conditions, which comprised 13 samples from three normal donors, were constructed. Fig. S1A shows the positive expression of CD73, CD90, CD105, and CD44 and negative expression of CD45, CD34, CD19, CD11b, CD79A, and HLA-DRA in the scRNA-seq data, confirming the reliability

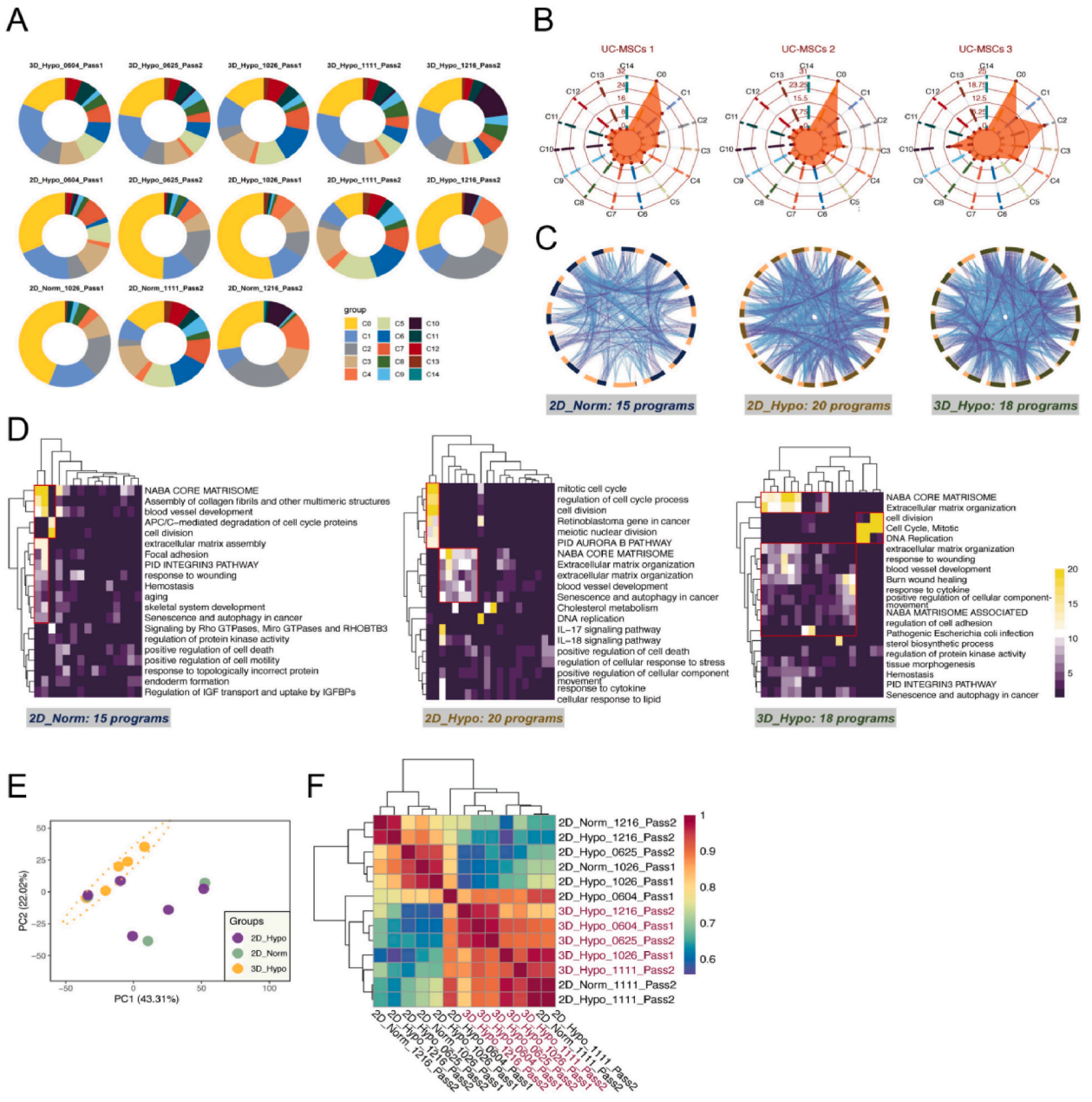

Fig. 4. TDHLSP system promotes more uniform distribution and closer relation of the MSC subpopulations. A: Cell proportion distribution of all 15 subpopulations in 13 samples using a pie chart. B: Radar plot displaying the heterogeneity of MSCs. C: Relationship among the NMF programs in the three cultured conditions. D: Enrichment analyses of different programs in the three cultured conditions illustrated in the heatmaps. E: Principal Component Analysis of all 13 samples. F: Correlation analyses among all 13 samples.

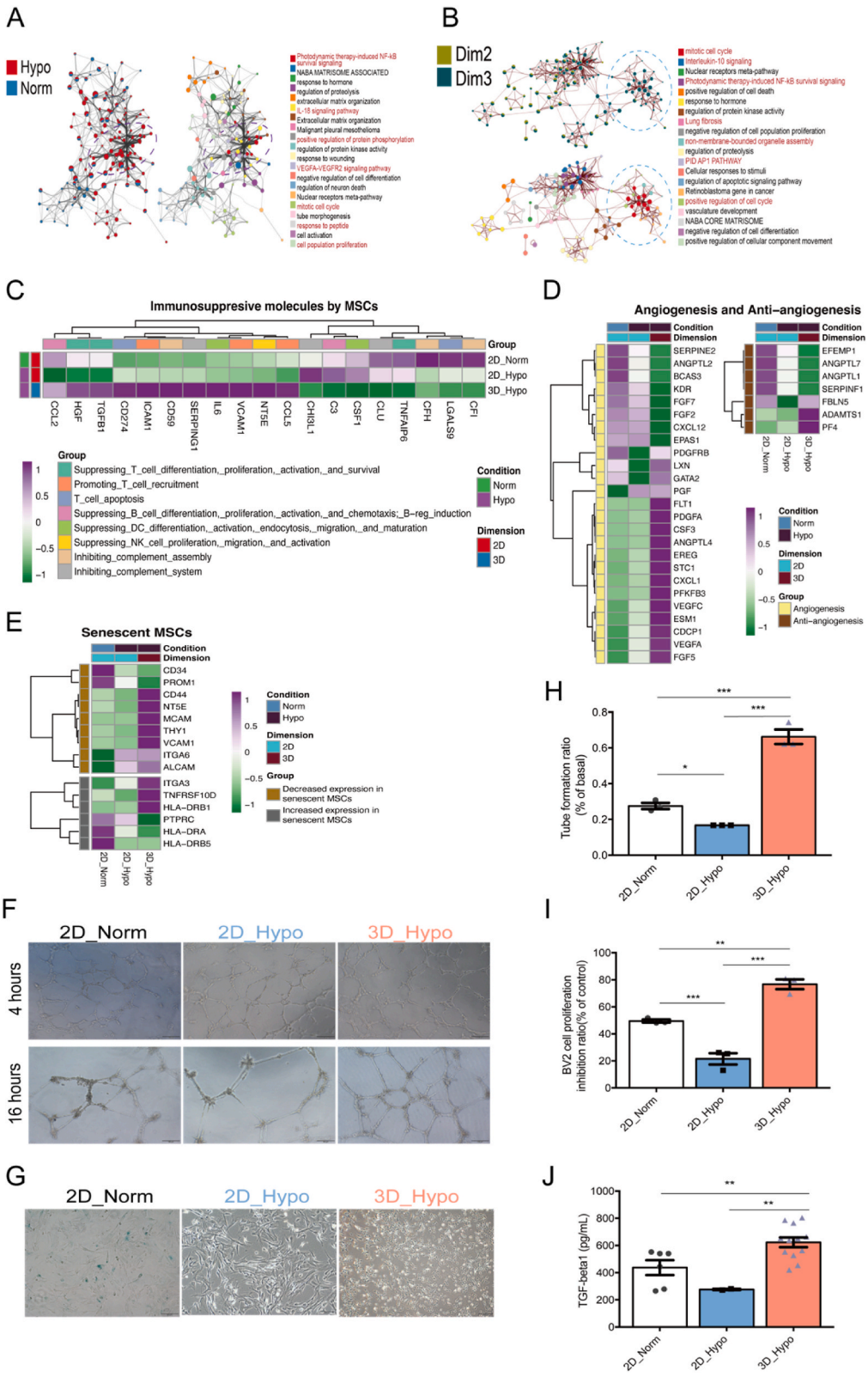

(caption on next page)

Fig. 5. TDHLSP system enhances the biological functions of 3D_Hypo MSCs. A: Enrichment analyses of differentially expressed genes between the Hypo and Norm or 2D and 3D condition. B: Enrichment analyses of the differentially expressed genes between 2D and 3D. C–E: Heatmap illustrating the expression of highly enriched DEGs based on the functional blocks related to angiogenesis and anti-angiogenesis (D), senescent MSCs (E), immunosuppression (C). Colour bar representing the relative gene expression. F: Tube formation assay using the culture supernatant from 2D and 3D cultured MSCs. Scale bar: 100 μm. G: Representative images of SA-β-gal staining in 2D and 3D cultured MSCs. Scale bar: 100 μm. H: Quantification of the tube formation ratio. n ≧ 3. One-Way ANOVA and Newman-Keuls Multiple Comparison Test. $*p < 0.05$, $***p < 0.001$. I: BV2 cell proliferation was inhibited by the supernatant of 2D and 3D cultured MSCs. n ≧ 3. One-Way ANOVA and Newman-Keuls Multiple Comparison Test. $**p < 0.01$, $***p < 0.001$. J: TGF-β1 secretion from the supernatant of 2D and 3D cultured MSCs. n ≧ 3. Student's t-test. $*p < 0.05$.

and cell state of the sequenced MSCs.

The analysis identified 15 clusters of MSCs based on the expression of highly variable genes (HVGs) across the total cell population, providing a visual representation of the diversity of the MSC subpopulations (Fig. 3A and B). The cell density was shown in Fig. 3C, which indicated that MSCs cultured in different conditions had different cell counts in each subpopulation. Notably, cells assigned to the G2/M and S phases constituted a substantial proportion of clusters 5, 6, 7, 11, and 12, indicating the competitive proliferative ability of these subpopulations (Fig. 3D). Moreover, the number of cells in clusters 5, 6, 7, 11, and 12 of the 3D_Hypo MSCs was proportionally larger than that of the 2D_Norm MSCs (Fig. 3D). It was approved by flow cytometry that more 3D MSCs stayed in G2/M and S phases than 2D MSCs (Fig. 3E), which suggesting an enhanced self-renewal ability attributed to culture in the TDHLSP system.

To further evaluate the functional pathways contributing to MSC heterogeneity, the DEGs of all 15 identified MSC clusters were classified into four main functional clusters. Notably, functional enrichment analysis revealed that the genes in hclust_1 were primarily associated with "collagen fibril organization", "extracellular matrix organization", and "cell adhesion". Furthermore, genes in hclust_2 and hclust_4 were predominantly enriched in "mitotic cell cycle", "cell cycle", "nuclear division", and "cell division", among other related processes. Interestingly, genes in hclust_3 were mainly associated with "blood vessel morphogenesis", "vasculature development", and "blood vessel development". Gene Set Enrichment Analysis (GSEA) revealed distinct distributions of mesenchyme and cell cycle scores, further emphasising the differences among the 15 MSC clusters. In summary, the major differences observed among the 15 clusters of MSCs can be categorised into two main functional groups: (1) cell cycle regulation and (2) extracellular matrix (ECM) (Fig. 3F). Then, the differentially-expressed genes in each cluster were shown in Fig. 3G and S3. Consistently, we found that the up-regulated genes in Cluster 5, 6, 7, 11, and 12 were highly similar and related to "Cell Cycle".

25.4. TDHLSP system promotes a more uniform distribution and closer relation of the MSC subpopulations

The heterogeneity of MSCs caused by differences in donors, tissue sources, and individual cells is recognised as a major factor contributing to the variable clinical efficacy of MSCs [31]. In this study, the distribution of the 15 clusters across the three donors was visualised using pie and radar charts, which revealed distinct subpopulation proportions for each donor (Fig. 4B). Notably, the 3D_Hypo MSCs exhibited a more even proportional distribution of clusters (Fig. 4A). NMF analysis was then employed to better understand the cell state under different culture conditions, which led to 15 programs from 2D_Norm MSCs, 20 from 2D_Hypo MSCs, and 18 from 3D_Hypo MSCs (Fig. 4C and D, Fig. S4). Enrichment analysis indicated that the programs of the 3D_Hypo MSCs were closely related (Fig. 4D). Furthermore, when the similarity among samples was analysed, the five samples of 3D_Hypo MSCs exhibited greater closeness to each other than to the other two conditions, which was consistent with the correlation analysis results (Fig. 4E and F). To confirm the observation of higher similarity and uniform distribution in the 3D_Hypo MSCs, the SCORPIUS package was used to reveal the potential pseudo-time distribution of all MSCs. Interestingly, based on the distribution calculated using SCORPIUS, the five scRNA samples from 3D_Hypo MSCs had a more effective overlap with each other than with the samples from the other two conditions (Fig. S5A). The gene heatmap following the estimated pseudotime of 3D_Hypo MSCs also had less variation than that of the other two culture conditions (Fig. S5B). In conclusion, the TDHLSP system promoted a more uniform distribution of MSC subpopulations, and donor differences were reduced. These findings have important implications for the standardisation and optimisation of MSC-based therapies.

25.5. The TDHLSP system enhances the biological functions of 3D_Hypo MSCs

In the exploration of the key components of the TDHLSP system, hypoxia and 3D culture, we opted to focus on understanding the variation in proteasome functional complexes in MSCs under these conditions. The t-value of the Gene Set Variation Analysis (GSVA) scores, computed using the GSVA package, highlighted significant differences in the signalling pathways between different cultured MSCs. Enrichment analysis of the DEGs revealed that hypoxic conditions upregulated the VEGFA-VEGFR2 signalling pathway, inflammatory signalling pathway (NF-κB and IL-18), and the cell population proliferation signalling pathway (Fig. 5A). In addition to the impact of oxygen levels, the 3D culture method markedly affects the mechanistic pathways of MSCs. Notable changes were observed in the cell cycle regulation pathway and related inflammatory signalling pathways, including NF-κB, IL-10, and PID AP1 signalling (Fig. 5B). Furthermore, analysis of the differences between 3D_Hypo MSCs from the MCB and the WCB revealed that only the "ECM proteoglycans" pathway differed among the top 20 enriched terms, suggesting a similar MSC state during passage (Fig. S5). In summary, the transcriptomic data indicated that both 3D culture and hypoxia may influence the biological functions of MSCs, potentially enhancing functions, such as angiogenesis and immunomodulation.

We proceeded to explore the differences in angiogenesis, immunosuppression, and anti-aging among the 2D_Norm, 2D_Hypo, and 3D_Hypo MSCs. First, we determined the average expression levels of angiogenesis-related, immunosuppression-related, and anti-

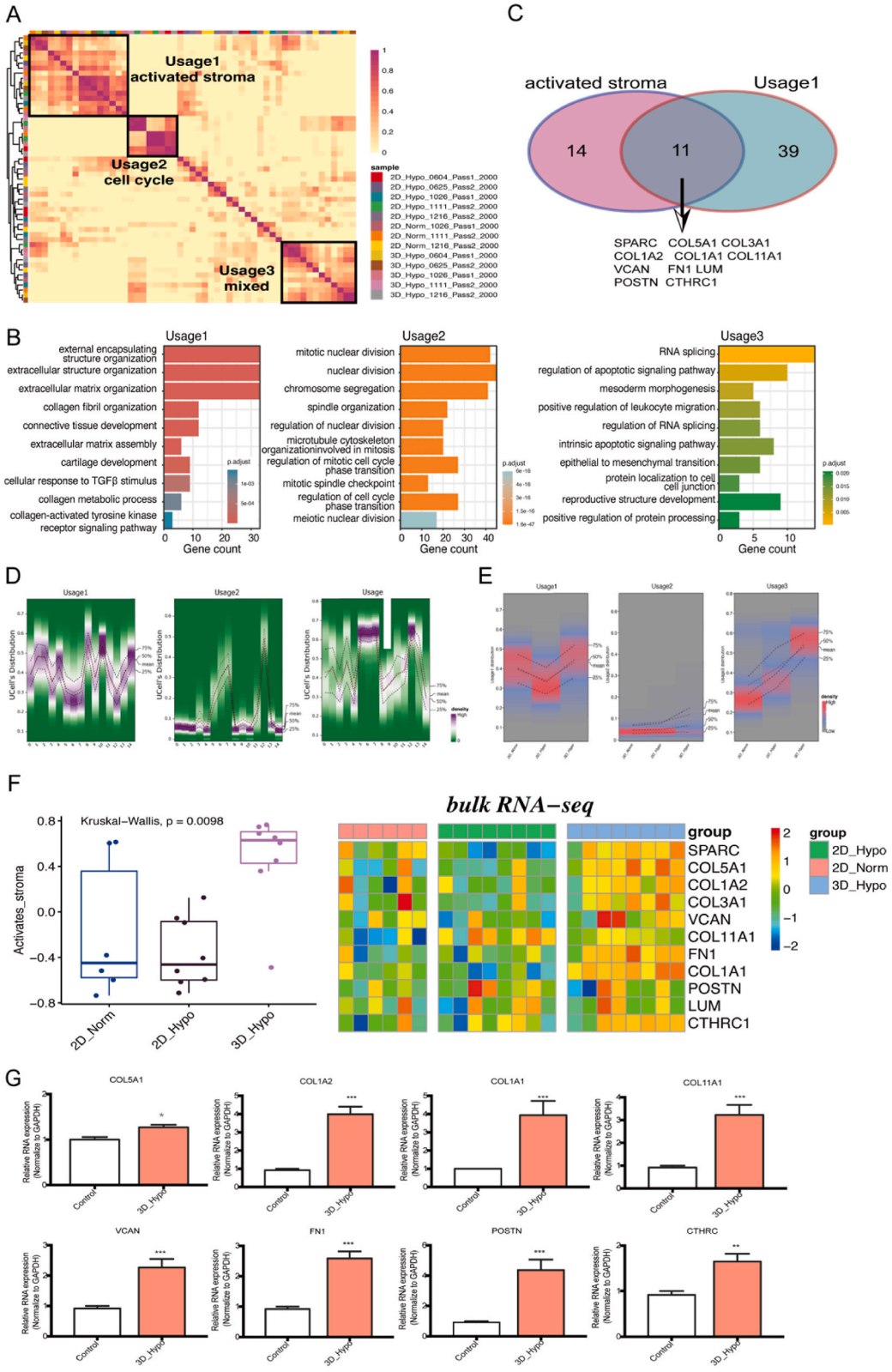

(caption on next page)

Fig. 6. Heterogeneity of MSCs is highly related to both "cell cycle" and "stroma." A: Correlation analysis for all identified programs of MSCs. B: Enrichment analysis of the three usages. The usages were identified based on the clustering results. C: Intersection of the top 50 genes in usage1 and the collected "activated stroma"-related genes. D: Scores of usages in 15 subpopulations. E: Scores of usages in the three culture conditions. F: Expression levels of the intersected genes in bulk RNAseq levels. G: mRNA levels of activated stroma-related genes (COL5A1, COL1A2, COL1A1, COL11A1, VCAN, FN1, POSTN, CTHRC) were determined using qRT-PCR (Control: 2D_Norm MSCs). n ≧ 3. Student's t-test. $*p < 0.05$, $**p < 0.01$, $***p < 0.01$.

aging-related genes based on pseudo-bulk RNA-seq data. Based on the results, 3D_Hypo MSCs may possess enhanced angiogenic, immunosuppressive, and anti-aging abilities (Fig. 5D, C, and 5E). To further assess the angiogenic capabilities, HUVECs were treated with the conditioned medium of MSCs from different groups. The imaging and quantitative results revealed that the conditioned medium of 3D_Hypo MSCs significantly promoted tube formation compared to that of 2D MSCs (Fig. 5F). The number of tubes in the

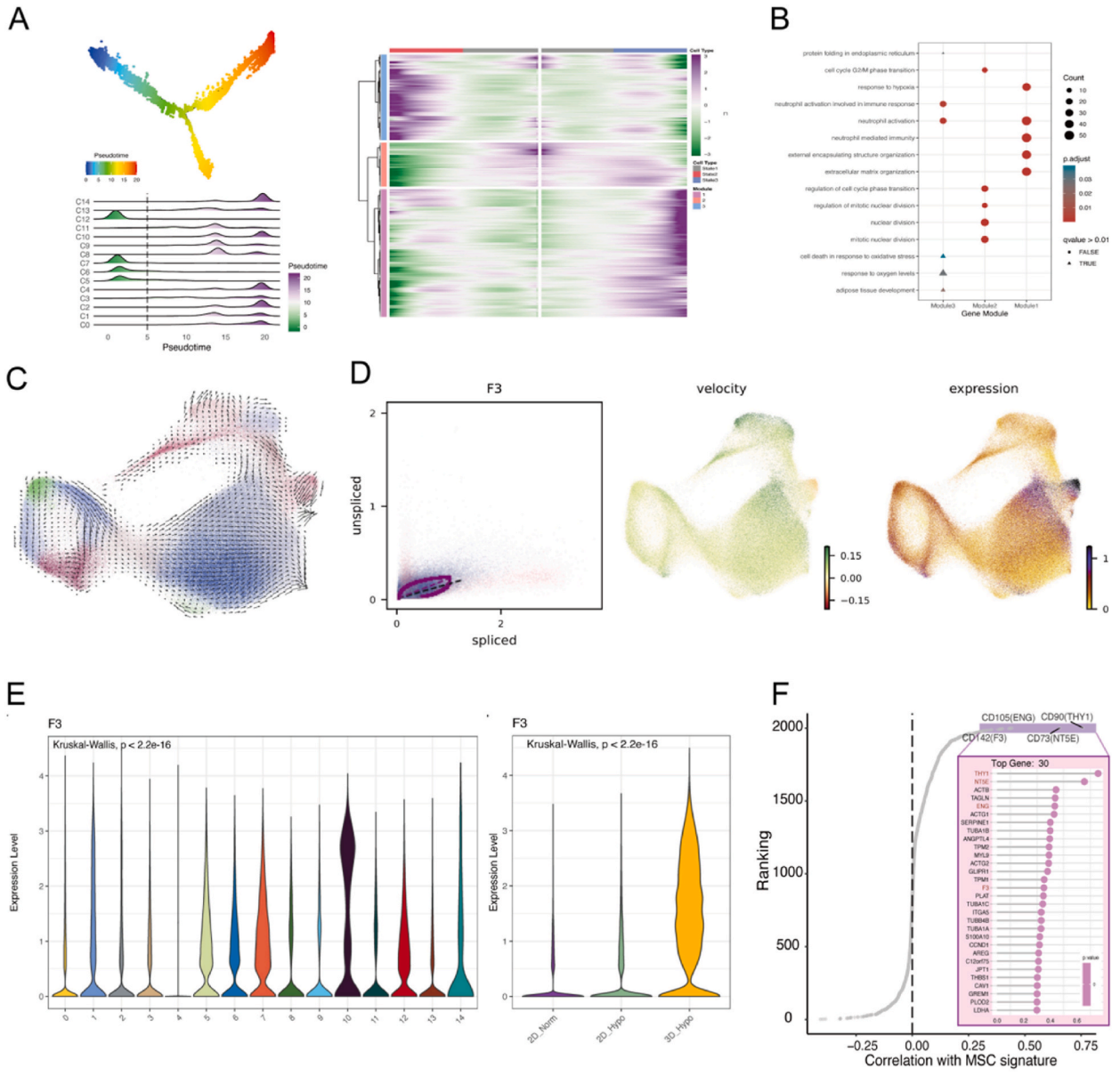

Fig. 7. CD142 is highly enriched in C10 subclusters and is a potential marker for 3D_Hypo MSCs. A: Trajectory analysis of MSCs and all 15 subpopulations. Heatmaps illustrating the genes with pseudotime-related changes and clustered in three modules. B: Enrichment analysis of the three pseudotime-related modules. C: RNA velocity results; the arrow indicates the pseudotime directions of each cell. D: Comparison of the unspliced and spliced mRNA of F3 (CD142) and the expression levels of CD142. E: Expression levels of CD142 in a violin plot. F: Correlation analysis of all genes with average expression of CD73, CD90, and CD105, the three markers of MSCs. The top 30 genes are enlarged.

2D_Hypo group was notably lower than that in the 2D_Norm group (Fig. 5H). In the senescence assay, several SA-β-gal-positive MSCs were observed in the 2D_Norm group, while MSCs in the 2D_Hypo and 3D_Hypo groups did not express SA-β-gal-positive cells (Fig. 5G). Although the 3D_Hypo MSCs demonstrated excellent immunomodulatory ability at the molecular level, further experiments are required. According to previous studies, MSCs suppress microglial proliferation [32]. Therefore, BV2 cells were co-cultured with conditioned medium from MSCs to assess immunosuppression in each group. Remarkably enhanced immunosuppression was observed with the conditioned medium of 3D_Hypo MSCs, leading to significant inhibition of BV2 cell proliferation compared to 2D-cultured MSCs. However, the proportion of BV2 cell proliferation inhibition in the 2D_Norm group was notably higher than that in the 2D_Hypo group (Fig. 5I). Furthermore, the cytokine, TGF-β1, which is known for its indispensable role in the immune system,

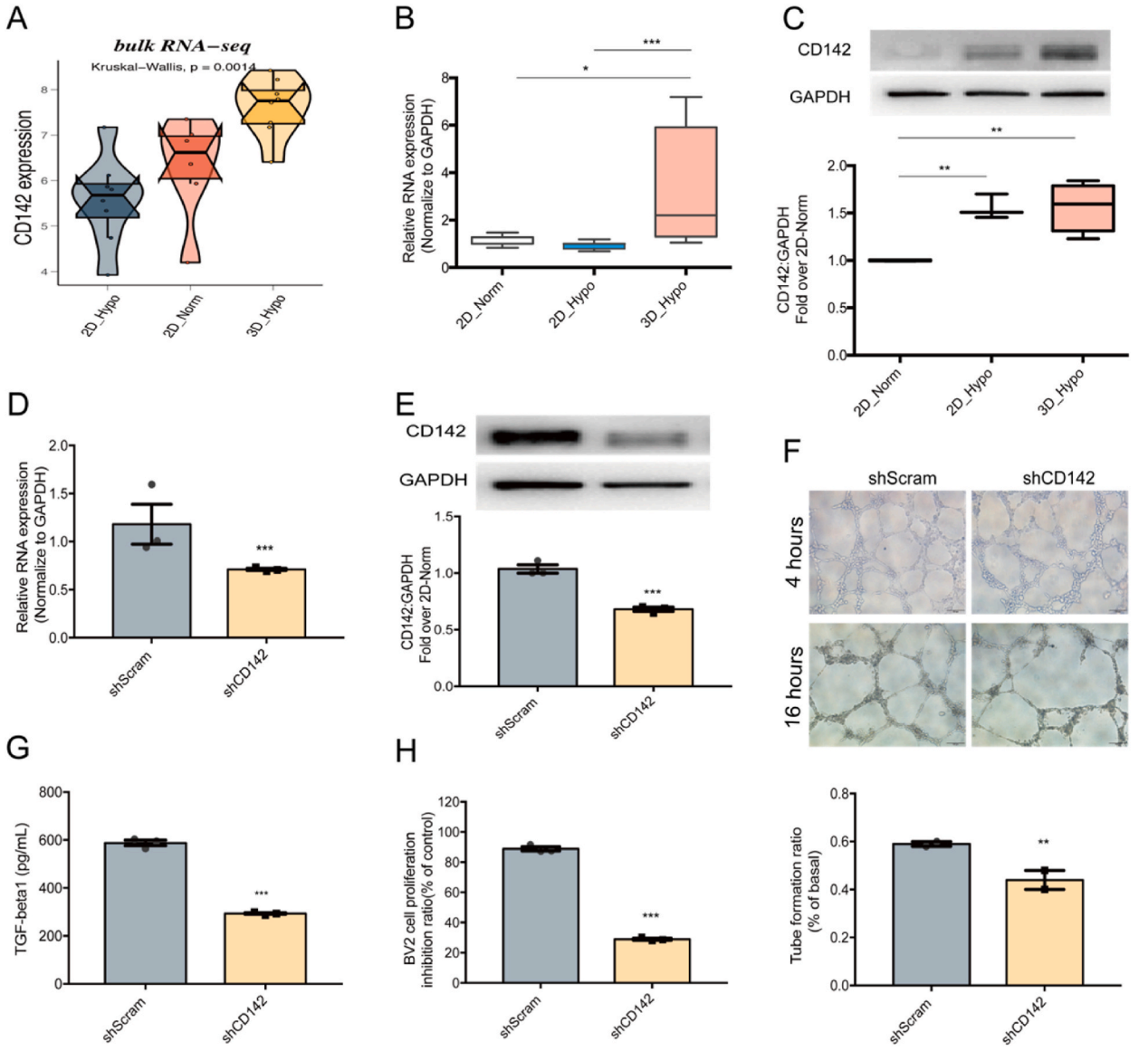

Fig. 8. Upregulation of CD142 in 3D_Hypo MSCs plays a major role in angiogenesis and immunomodulatory capacity. A: Expression levels of CD142 in the three culture conditions of MSCs based on bulk RNAseq. B: mRNA expression of CD142 for 2D and 3D cultured MSCs based on qRT-PCR. n ≧ 3. One-Way ANOVA and Newman-Keuls Multiple Comparison Test. $*p < 0.05$, $***p < 0.001$. C: Protein levels of CD142 for 2D and 3D cultured MSCs based on Western blot. GAPDH was used as a control (n = 3). One-Way ANOVA and Newman-Keuls Multiple Comparison Test. $**p < 0.01$. **D**: CD142 mRNA expression in CD142 knockdown 3D_Hypo MSCs. 3D_Hypo MSCs were transfected with the shCD142 lentiviral vector to knockdown CD142. 3D_Hypo MSCs transfected with the PLKO.1 vector served as the shScram group. GAPDH was used as a control (n = 3). Student's t-test. $***p < 0.001$. E: Validation of the CD142 protein in CD142 knockdown 3D_Hypo MSCs. n ≧ 3. Student's t-test. $***p < 0.001$. F: Tube formation assay using the culture supernatant from shCD142 and shScram of 3D_Hypo MSCs. Scale bar: 100 μm. Quantification of tube formation ratio. n ≧ 3. Student's t-test. $**p < 0.01$. G: TGF-β1 secretion from the supernatant of shCD142 and shScram of 3D_Hypo MSCs. n ≧ 3. Student's t-test. $***p < 0.001$. H: BV2 cell proliferation was inhibited by the supernatant of shCD142 and shScram of 3D_Hypo MSCs. n ≧ 3. Student's t-test. $***p < 0.001$.

including the inhibition of T cell proliferation [33], induction of regulatory T cells (Tregs), and modulation of microglial activation [34], may play a key role in the observed immunomodulatory effects. Based on the ELISA results, 3D_Hypo MSCs secreted significantly higher levels of TGF-β1 than 2D-cultured MSCs. In addition, the level of TGF-β1 in the 2D_Hypo group was remarkably decreased relative to that in the 2D_Norm group (Fig. 5J). These findings further validate that 3D_Hypo MSCs are comparatively younger and exhibit better potential for angiogenesis and immunomodulation than 2D_Hypo MSCs.

25.6. NMF analysis further confirms that the heterogeneity of MSCs is highly related to both "cell cycle" and "stroma"

In the NMF analysis, 3D_Hypo MSCs exhibited less heterogeneity than the other two MSCs. To gain further insights into the main functions of all identified programs under the three conditions, a correlation analysis among all programs was conducted, revealing three usages (Fig. 6A). Based on enrichment analysis of these usages, these usages were named Usage1, 2, and 3, representing "activated stroma", "cell cycle", and "mixture of both activated stroma and cell cycle", respectively (Fig. 6B). Notably, the name "activated stroma" was assigned because the genes in Usage1 intersected with the "activated stroma" genes collected from Moffitt et al. [35] (Fig. 6C). Therefore, this NMF analysis further confirmed that the heterogeneity of MSCs is mainly and remarkably related to "stroma/mesenchyme" and "cell cycle." The ssGSEA algorithm was employed to calculate the usage scores. Usages 2 and 3 were mainly enriched in proliferative subpopulations 5, 6, 7, and 12, whereas Usage 1 contributed to the other MSC subpopulations (Fig. 6D). Importantly, all three usage scores were significantly activated in 3D_Hypo MSCs compared to those in the other two conditions, indicating better MSC characteristics (Fig. 6E). Using the ssGSEA algorithm, the signature score of "activated stroma" was calculated. Notably, 3D_Hypo MSCs were found to possess a higher score than cells subjected to the other two conditions, indicating the "activated stroma" state of 3D_Hypo MSCs (Fig. 6F). Subsequently, qRT-PCR confirmed the higher expression of activated stromal genes in 3D_Hypo MSCs, including COL5A1, COL1A2, POSTN, COL1A1, COL11A1, VCAN, FN1, and CTHRC (Fig. 6G).

25.7. CD142 is highly enriched in C10 subclusters and identified as a potential marker for 3D_Hypo MSCs

To further uncover potentially crucial genes or subpopulations of MSCs, we performed trajectory analysis (Fig. 7A). We also conducted an enrichment analysis of the pseudo-time-related genes in modules 1, 2, and 3 based on the monocle 2 package [36]. Consistent with the above results, the biological functions of gene modules were mainly related to cell cycle at the root of pesudotime and finally related to mesenchyme/ECM/stroma (Fig. 7B). To further validate these findings, the RNA velocity algorithm was applied, and the pipeline was executed for each MSC sample (Fig. 7C and S7). Interestingly, RNA velocity analysis revealed that the five samples from 3D_Hypo MSCs exhibited markedly more uniform changes than cells subjected to the other two culture conditions. In particular, the pseudotime changes between each cluster were more regular in the 3D_Hypo MSCs than the other cells (Fig. S7).

Of note, CD142 was more highly expressed following pseudotime and was markedly expressed at the end of the pseudotime in most samples, indicating the potentially crucial role of CD142 (Fig. 7D). CD142, also known as F3, is a wound healing marker in MSCs [35]. The expression levels of CD142 were examined based on previous findings. Interestingly, CD142 was highly expressed in cluster 10, the terminus of the inferred pseudotime, and in 3D_Hypo MSCs, consistent with the results of bulk scRNA-seq (Fig. 7E). A correlation analysis was also performed to rank all genes based on the average expression of CD73, CD90, and CD105. Notably, CD142 was one of the most highly expressed genes (Fig. 7F). Furthermore, when the expression levels of biological function genes were compared among the 15 clusters, cluster 10 was found to possess more biological functions, including angiogenesis, immunosuppression, and anti-senescence (Fig. S8). In summary, CD142 was highly enriched in the cluster 10 subcluster and was identified as a potential marker of 3D_Hypo MSCs.

25.8. Upregulation of CD142 in 3D_Hypo MSCs plays a major role in angiogenesis and immunomodulatory capacity

Bulk RNA-seq analysis confirmed the high expression of CD142 in 3D_Hypo MSCs (Fig. 8A). qRT-PCR and Western blot assays consistently revealed a significant upregulation of CD142 in 3D_Hypo MSCs (Fig. 8B and C). Previous studies have emphasised the potential importance of CD142 in the biological functions of MSCs. For instance, $CD142^{+}$ MSCs are associated with wound healing potential [35], and CD142 may serve as a biomarker of the ability of MSCs to promote wound healing [37]. The functional role of CD142 in immunoregulation was explored by generating a stable CD142 knockdown MSC line using an shCD142 lentiviral vector in 3D_Hypo MSCs. The efficiency of knockdown was confirmed using qRT-PCR and Western blot assays, which revealed a significant decrease in both the mRNA and protein expression of CD142 in the shCD142 group (Fig. 8D and E). Functional assays were performed to assess the effect of CD142 knockdown. The conditioned medium from the shCD142 group was found to significantly inhibit tube formation (Fig. 8F), suggesting that CD142 enrichment in 3D_Hypo MSCs might contribute to the promotion of angiogenesis. Regarding immunomodulation capability, the amount of TGF-β1 decreased after CD142 downregulation (Fig. 8G). Similarly, the ratio of BV2 cell proliferation inhibition decreased in the shCD142 group compared to that in the shScram group (Fig. 8H). In summary, these results indicate that CD142 plays a role in regulating the abilities related to angiogenesis and immunomodulation in 3D_Hypo MSCs.

26. Discussion

This study aimed to develop an automated, closed, and scalable method for MSCs using a quality control system. In addition, the properties and transcriptomes of 3D_Hypo MSCs were explored. We established a TDHLSP platform with matched quality assessment

to produce GMP-grade MSCs. Initially, an average of 2×10^8 MSCs (P3) were seeded; however, after 5 days, 2.4×10^9 3D_Hypo MSCs were harvested, with a total of 4.6×10^9 obtained on day 10. The system includes four levels of cell banks, and the cells from each bank are qualified. The properties and safety of 3D_Hypo MSCs were determined by assessing the presence of viruses, surface markers, sterility, mycoplasma, STR, tumourigenicity, and trilineage differentiation. Comparison of the single-cell transcriptome sequencing of 3D_Hypo MSCs with 2D cultured MSCs revealed that the heterogeneity of MSCs was markedly related to both "cell cycle" and "stroma/mesenchyme", with 3D_Hypo MSCs expressing higher activated stroma genes. Notably, the subgroup distribution of 3D_Hypo MSCs was more uniform than that of 2D MSCs. Vascularisation and immunosuppressive abilities were significantly increased in 3D_Hypo MSCs, and the cells appeared younger. Furthermore, 3D_Hypo MSCs stably expressed higher levels of CD142, while tube formation and immunoregulation abilities were lower in 3D_Hypo MSCs with CD142 knockdown. These results suggest that 3D_Hypo MSCs have competitive clinical potential due to their higher yield, better biological functions, and more uniform cell subset distribution. These preliminary findings indicate that the enrichment of CD142 might be the main regulatory molecule for the function of 3D_Hypo MSCs.

In previous studies on the yield of MSC microcarrier culture, Zhang et al. reported that 1.5×10^8 cells were cultured in a 5 L bioreactor for 4 days, resulting in the production of 2.2×10^9 cells [38]. Based on our study, culturing 2×10^8 cells in a 2.6 L TDHLSP bioreactor under 3D and hypoxic conditions for 5 days resulted in cell expansion to 2.4×10^9 cells. The microcarriers in the bioreactor provided an ample adhesive surface area for MSCs in the 3D suspension, enabling large-scale cell expansion in a relatively small volume of culture medium. The TDHLSP system simulates the natural environment in which MSCs survive *in vivo* [39]. Notably, interactions between MSCs and realistic biochemical and physiological reactions were preserved in this culture mode. In addition, the suspension system facilitated enhanced nutrient intake and gas exchange. In a 3D hypoxic environment, MSCs respond more actively to both endogenous and exogenous stimuli, such as changes in temperature, pH, nutrient absorption, transport, and differentiation [40]. Hence, a significant room exists for optimising the MSC expansion efficiency using bioreactor cultivation methods. In the future, the cell expansion efficiency could be enhanced by modifying the culture process, such as altering the feeding methods, culture volume, or duration. In summary, variations in initial cell characteristics, microcarrier properties, culture medium composition, process parameters, and culture conditions may contribute to differences in cell expansion levels [41].

The 3D_Hypo MSCs maintained typical MSC characteristics. Interestingly, the 3D_Hypo MSCs were smaller and had a shorter cell diameter than the 2D MSCs. Mizukami et al. observed a reduction in the expression of CD105 (55 ± 7.5 %), a slight increase in endothelial cell markers (CD31) in MSCs, and elevated levels of HLA-DR after bioreactor expansion [20]. Similarly, TDHLSP resulted in a non-significant increase in the expression of CD11b, CD19, CD31, CD34, CD45, and HLA-DR in MSCs and a slight decrease in CD105 (95.9 %) expression. According to several studies, the three-directional differentiation potential of 3D MSCs is comparable to that of 2D MSCs [20]. However, Egger et al. reported a slight increase in adipogenesis and chondrogenesis, and a decrease in the osteogenic differentiation of MSCs under hypoxic conditions compared with normoxic conditions [22]. Nevertheless, our study revealed that 3D_Hypo MSCs differentiated into more osteocytes and fewer adipocytes than 2D MSCs. We speculate that these changes in MSCs may be attributed to shear stress in the reactor or enzymatic digestion [20,21].

scRNA-seq revealed enhanced proliferative capacity of 3D_Hypo MSCs compared with that of 2D MSCs. These findings align with those of previous studies. Zhang et al. suggested that microcarrier-expanded hUC-MSCs exhibit increased proliferation ability and reduced cell numbers in the delayed phase of the cell cycle [15]. According to several reports, low oxygen gradient or hypoxic conditions promote cell proliferation. In particular, hypoxia is reported to induce a steady increase in intracellular HIF-1α, subsequently impacting Notch and Wnt/β-catenin signalling —proteins known to strongly influence proliferation [42].

The heterogeneity of MSCs depends on their origin, such as their biological niche, or donor characteristics, including age and disease status [43]. In our study, MSC heterogeneity was closely associated with the ECM and cell cycle based on enrichment analysis of the top genes and NMF analysis. Conversely, other studies suggest that MSC heterogeneity is strongly linked to their entry into the G2/M phase [44] or ECM composition [31]. In clinical applications, the heterogeneity of MSCs poses challenges to achieving stable therapeutic efficacy, leading to difficulties in obtaining consistent clinical data [43,45]. Intriguingly, the distribution of clusters in 3D_Hypo MSCs was more uniform, and a higher correlation was found between cell clusters relative to those of 2D-cultured MSCs. We hypothesised that MSCs from different sources may become synchronised after preconditioning under 3D and hypoxic conditions.

Based on enrichment analysis, hypoxic conditions upregulated signalling pathways, including VEGFA-VEGFR2, NF-κB, IL-18, and the cell cycle. 3D culture also induced cell cycle regulation and related inflammatory signalling pathways, such as NF-κB, IL-10, and PID-AP1. These findings suggest that the functionalities of MSCs cultured in 3D and hypoxic environments were superior to those of MSCs cultured in 2D. By further analysing genes associated with angiogenesis, immunosuppression, and anti-aging, we observed an increase in their expression in 3D_Hypo MSCs, which was subsequently verified using *in vitro* experiments. Previous studies revealed that the capacity to induce angiogenesis is VEGFR2-dependent in stem cells [46]. Moreover, modulating the Notch/NF-κB signals can promote paracrine activity of BMSCs to enhance angiogenesis [47].

We investigated the main functional cell populations and key functional molecules in the 3D_Hypo MSCs. 3D_Hypo MSCs were primarily concentrated in subgroups 11, 12, and 10. Subgroup C10 had high expression levels of genes related to vascular repair. The paracrine activity of MSCs, which stimulates angiogenesis and recruits local stem cells, involves the secretion of VEGF-A [48], F3 [49], TGFB1 [50], and CCL2 [51]. Our scRNA-seq data revealed that numerous genes related to angiogenesis were highly enriched in subgroup C10, indicating their close association with the regenerative capacity of 3D_Hypo MSCs.

CD142 was found to be overexpressed in 3D_Hypo MSCs. $S100A9^+CD29^+CD142^+$ MSCs were reported to have beneficial effects on wound healing cells (keratinocytes/fibroblasts/endothelial cells), thereby promoting cell proliferation and migration [37]. To further confirm the key function of CD142, we conducted CD142 knockdown experiments in 3D_Hypo MSCs. CD142 knockdown resulted in decreased secretion of TGF-β1, inhibition of BV2 cell proliferation, and reduced blood tube formation. These findings suggest that CD142 is an important functional molecule in 3D_Hypo MSCs and is closely related to their angiogenic and immunomodulatory

capacities.

Taken together, we hypothesised that the two culture conditions of TDHLSP (hypoxia and 3D) might trigger HIF-1α, subsequently activating the VEGFA-VEGFR2 and NF-κB signalling pathways to enhance the biological functions of 3D_Hypo MSCs by enriching CD142. Nevertheless, these results must be interpreted with caution given the limitations of our current understanding of the mechanisms involved. Further studies are required to investigate the specific role of CD142 in the functional mechanisms of 3D_Hypo MSCs. We sought to reveal the biomarkers, regulatory pathways, and mechanisms related to the functionality of 3D_Hypo MSCs to provide scientific evidence and a theoretical basis for the clinical research and translational applications of MSCs.

This study had a few limitations. First, the TDHLSP system must be used in a GMP environment to avoid cell contamination throughout the production process. Further, only MSCs produced using specific parameters were analysed. According to changes in conditions, such as oxygen concentration, glucose concentration, pH, and culture time, cell growth status, cell number, and gene expression may differ. In a specific production process, the producer must continuously adjust the process to adapt to production needs. In the follow-up, we will conduct an in-depth study to determine the therapeutic effects of MSCs cultured using the TDHLSP system in animal models; the role of CD142 in the function of MSCs cultured in 3D; and other factors that may affect their function. Further studies on the effect of 3D culture conditions on MSC function and optimisation of culture parameters are needed to further improve cell function.

27. Conclusions

In this study, we established a TDHLSP platform for industrial production of MSCs. The 3D_Hypo MSCs expanded using the TDHLSP device met the CQA requirements of MSCs and exhibited competitive biological properties. Furthermore, culture using the TDHLSP system promoted even distribution of 3D_Hypo MSCs. The enrichment of CD142 in 3D_Hypo MSCs may be involved in the regulation of cellular functions. These findings support the establishment of a large-scale, automated, and efficient stem cell *in vitro* expansion system, which represents a significant advancement in stem cell clinical applications.

Abbreviations

TDHLSP	Three-dimensional hypoxic large-scale production
MSCs	Mesenchymal stem cells
GMP	Good Manufacturing Practice
2D	Two-dimensional
3D	Three-dimensional
shRNA	short hairpin RNA
3D_Hypo MSCs	3D and hypoxic cultured mesenchymal stem cells
2D_Hypo MSCs	2D and hypoxic cultured mesenchymal stem cells
2D_Norm MSCs	2D and normoxic cultured mesenchymal stem cells
scRNA-seq	Single cell RNA-sequencing
UMAP	Uniform manifold approximation and projection
PCA	Principal component analysis
DEGs	Differentially expressed genes
HVGs	Dighly variable genes
OD	Optical density
PFA	Paraformaldehyde
SCENIC	Single-cell regulatory network inference and clustering
TF	Transcription factors
NMF	Non-negative matrix factorization
TRAP	Telomeric repeat amplification protocol
HSF	Human skin fibroblasts
iPSC	Human induced pluripotent stem cell
qRT-PCR	Quantitative real-time polymerase chain reaction
STR	Short tandem repeat
ELISA	Enzyme-linked immunosorbent assay
SA-β-gal	Senescence-associated-β-galactosidase
P1	Passage 1
P3	Passage 3
MCB	Master cell bank
WCB	Work cell bank
Cell Bank	CB
CQA	Critical quality attributes
GSEA	Gene set enrichment analysis
ECM	Extracellular matrix
IND	Investigational New Drug
R&D	Research&Development
HUVECs	Human umbilical vein endothelial cells
Tregs	Regulatory T cells

Data availability statement

Data relevant to our research are not deposited in publicly available repositories. The data will be made available on request.

Funding

This work was funded by the study on the standardized and large scale production and the quality assessment of stem cell therapy products, Major Program of the National Key Research and Development Project (Grant# 2020YFA0112602), the Peak Disciplines (Type IV) of Institutions of Higher Learning in Shanghai, and the Shanghai Collaborative Innovation Program on Regenerative Medicine and Stem Cell Research (Grant# 2019CXJQ01).

Ethics approval and consent to participate

This study did not involve any human samples and was approved by the Ethics Committee of Shanghai East Hospital of Tongji University.

CRediT authorship contribution statement

Yiyao Qi: Writing – review & editing, Writing – original draft, Methodology, Data curation. **Xicheng Wang:** Writing – review & editing, Writing – original draft, Formal analysis, Data curation. **Zhihui Bai:** Writing – review & editing, Writing – original draft. **Ying Xu:** Writing – review & editing, Conceptualization. **Tingting Lu:** Resources, Conceptualization. **Hanyu Zhu:** Validation. **Shoumei Zhang:** Validation. **Zhihong Wu:** Validation. **Zhongmin Liu:** Funding acquisition. **Zhiying He:** Writing – review & editing, Funding acquisition. **Wenwen Jia:** Writing – review & editing, Funding acquisition.

Declaration of competing interest

The authors declare that they have no known competing financial interests or personal relationships that could have appeared to influence the work reported in this paper.

Acknowledgment

We gratefully acknowledge the Nanjing Birui Biotechnology Co., Ltd for co-developing TDHLSP system.

Appendix A. Supplementary data

Supplementary data to this article can be found online at https://doi.org/10.1016/j.heliyon.2024.e30968.

References

[1] H. Lin, J. Sohn, H. Shen, M.T. Langhans, R.S. Tuan, Bone marrow mesenchymal stem cells: aging and tissue engineering applications to enhance bone healing, Biomaterials 203 (2019) 96–110, https://doi.org/10.1016/j.biomaterials.2018.06.026.
[2] N.H. Riordan, I. Morales, G. Fernandez, N. Allen, N.E. Fearnot, M.E. Leckrone, D.J. Markovich, D. Mansfield, D. Avila, A.N. Patel, et al., Clinical feasibility of umbilical cord tissue-derived mesenchymal stem cells in the treatment of multiple sclerosis, J. Transl. Med. 16 (1) (2018) 57, https://doi.org/10.1186/s12967-018-1433-7.
[3] Y. Kuang, X. Zheng, L. Zhang, X. Ai, V. Venkataramani, E. Kilic, D.M. Hermann, A. Majid, M. Bahr, T.R. Doeppner, Adipose-derived mesenchymal stem cells reduce autophagy in stroke mice by extracellular vesicle transfer of miR-25, J. Extracell. Vesicles 10 (1) (2020) e12024, https://doi.org/10.1002/jev2.12024.
[4] H.J. Kim, K.R. Cho, H. Jang, N.K. Lee, Y.H. Jung, J.P. Kim, J.I. Lee, J.W. Chang, S. Park, S.T. Kim, et al., Intracerebroventricular injection of human umbilical cord blood mesenchymal stem cells in patients with Alzheimer's disease dementia: a phase I clinical trial, Alzheimer's Res. Ther. 13 (1) (2021) 154, https://doi.org/10.1186/s13195-021-00897-2.
[5] T. Lan, M. Luo, X. Wei, Mesenchymal stem/stromal cells in cancer therapy, J. Hematol. Oncol. 14 (1) (2021) 195, https://doi.org/10.1186/s13045-021-01208-w.
[6] A. Naji, M. Eitoku, B. Favier, F. Deschaseaux, N. Rouas-Freiss, N. Suganuma, Biological functions of mesenchymal stem cells and clinical implications, Cell. Mol. Life Sci. 76 (17) (2019) 3323–3348, https://doi.org/10.1007/s00018-019-03125-1.
[7] Y. Han, X. Li, Y. Zhang, Y. Han, F. Chang, J. Ding, Mesenchymal stem cells for regenerative medicine, Cells 8 (8) (2019), https://doi.org/10.3390/cells8080886.
[8] N. Watson, R. Divers, R. Kedar, A. Mehindru, A. Mehindru, M.C. Borlongan, C.V. Borlongan, Discarded Wharton jelly of the human umbilical cord: a viable source for mesenchymal stromal cells, Cytotherapy 17 (1) (2015) 18–24, https://doi.org/10.1016/j.jcyt.2014.08.009.
[9] L.X. Guan, H. Guan, H.B. Li, C.A. Ren, L. Liu, J.J. Chu, L.J. Dai, Therapeutic efficacy of umbilical cord-derived mesenchymal stem cells in patients with type 2 diabetes, Exp. Ther. Med. 9 (5) (2015) 1623–1630, https://doi.org/10.3892/etm.2015.2339.
[10] Q. Xie, R. Liu, J. Jiang, J. Peng, C. Yang, W. Zhang, S. Wang, J. Song, What is the impact of human umbilical cord mesenchymal stem cell transplantation on clinical treatment? Stem Cell Res. Ther. 11 (1) (2020) 519, https://doi.org/10.1186/s13287-020-02011-z.
[11] Y. Gu, T. Li, Y. Ding, L. Sun, T. Tu, W. Zhu, J. Hu, X. Sun, Changes in mesenchymal stem cells following long-term culture in vitro, Mol. Med. Rep. 13 (6) (2016) 5207–5215, https://doi.org/10.3892/mmr.2016.5169.
[12] A.K. Chen, S. Reuveny, S.K. Oh, Application of human mesenchymal and pluripotent stem cell microcarrier cultures in cellular therapy: achievements and future direction, Biotechnol. Adv. 31 (7) (2013) 1032–1046, https://doi.org/10.1016/j.biotechadv.2013.03.006.

[13] A.S. Simaria, S. Hassan, H. Varadaraju, J. Rowley, K. Warren, P. Vanek, S.S. Farid, Allogeneic cell therapy bioprocess economics and optimization: single-use cell expansion technologies, Biotechnol. Bioeng. 111 (1) (2014) 69–83, https://doi.org/10.1002/bit.25008.
[14] E. Tomecka, W. Lech, M. Zychowicz, A. Sarnowska, M. Murzyn, T. Oldak, K. Domanska-Janik, L. Buzanska, N. Rozwadowska, Assessment of the Neuroprotective and Stemness properties of human Wharton's jelly-derived mesenchymal stem cells under variable (5% vs. 21%) Aerobic conditions, Cells 10 (4) (2021), https://doi.org/10.3390/cells10040717.
[15] X. Wang, L. Ouyang, W. Chen, Y. Cao, L. Zhang, Efficient expansion and delayed senescence of hUC-MSCs by microcarrier-bioreactor system, Stem Cell Res. Ther. 14 (1) (2023) 284, https://doi.org/10.1186/s13287-023-03514-1.
[16] X. Yan, K. Zhang, Y. Yang, D. Deng, C. Lyu, H. Xu, W. Liu, Y. Du, Dispersible and dissolvable Porous microcarrier Tablets enable efficient large-scale human mesenchymal stem cell expansion, Tissue Eng. C Methods 26 (5) (2020) 263–275, https://doi.org/10.1089/ten.TEC.2020.0039.
[17] T.J. Bartosh, J.H. Ylostalo, A. Mohammadipoor, N. Bazhanov, K. Coble, K. Claypool, R.H. Lee, H. Choi, D.J. Prockop, Aggregation of human mesenchymal stromal cells (MSCs) into 3D spheroids enhances their antiinflammatory properties, Proc. Natl. Acad. Sci. U. S. A. 107 (31) (2010) 13724–13729, https://doi.org/10.1073/pnas.1008117107.
[18] S. Gao, Y. Jin, J. Ma, J. Wang, J. Wang, Z. Shao, T. Fan, M. Zhang, D. Chang, Preclinical study of human umbilical cord mesenchymal stem cell sheets for the recovery of ischemic heart tissue, Stem Cell Res. Ther. 13 (1) (2022) 252, https://doi.org/10.1186/s13287-022-02919-8.
[19] T. Nicotra, A. Desnos, J. Halimi, H. Antonot, L. Reppel, T. Belmas, A. Freton, F. Stranieri, M. Mebarki, J. Larghero, et al., Mesenchymal stem/stromal cell quality control: validation of mixed lymphocyte reaction assay using flow cytometry according to ICH Q2(R1), Stem Cell Res. Ther. 11 (1) (2020) 426, https://doi.org/10.1186/s13287-020-01947-6.
[20] A. Mizukami, A. Fernandes-Platzgummer, J.G. Carmelo, K. Swiech, D.T. Covas, J.M. Cabral, C.L. da Silva, Stirred tank bioreactor culture combined with serum-/xenogeneic-free culture medium enables an efficient expansion of umbilical cord-derived mesenchymal stem/stromal cells, Biotechnol. J. 11 (8) (2016) 1048–1059, https://doi.org/10.1002/biot.201500532.
[21] F. Santos, P.Z. Andrade, M.M. Abecasis, J.M. Gimble, L.G. Chase, A.M. Campbell, S. Boucher, M.C. Vemuri, C.L. Silva, J.M. Cabral, Toward a clinical-grade expansion of mesenchymal stem cells from human sources: a microcarrier-based culture system under xeno-free conditions, Tissue Eng. C Methods 17 (12) (2011) 1201–1210, https://doi.org/10.1089/ten.tec.2011.0255.
[22] D. Egger, I. Schwedhelm, J. Hansmann, C. Kasper, Hypoxic three-dimensional Scaffold-free aggregate cultivation of mesenchymal stem cells in a stirred tank reactor, Bioengineering (Basel) 4 (2) (2017), https://doi.org/10.3390/bioengineering4020047.
[23] M. Dominici, K. Le Blanc, I. Mueller, I. Slaper-Cortenbach, F. Marini, D. Krause, R. Deans, A. Keating, D. Prockop, E. Horwitz, Minimal criteria for defining multipotent mesenchymal stromal cells. The International Society for Cellular Therapy position statement, Cytotherapy 8 (4) (2006) 315–317, https://doi.org/10.1080/14653240600855905.
[24] B. Dura, J.Y. Choi, K. Zhang, W. Damsky, D. Thakral, M. Bosenberg, J. Craft, R. Fan, scFTD-seq: freeze-thaw lysis based, portable approach toward highly distributed single-cell 3' mRNA profiling, Nucleic Acids Res. 47 (3) (2019) e16, https://doi.org/10.1093/nar/gky1173.
[25] Y. Liao, G.K. Smyth, W. Shi, featureCounts: an efficient general purpose program for assigning sequence reads to genomic features, Bioinformatics 30 (7) (2014) 923–930, https://doi.org/10.1093/bioinformatics/btt656.
[26] Y. Zhou, B. Zhou, L. Pache, M. Chang, A.H. Khodabakhshi, O. Tanaseichuk, C. Benner, S.K. Chanda, Metascape provides a biologist-oriented resource for the analysis of systems-level datasets, Nat. Commun. 10 (1) (2019) 1523, https://doi.org/10.1038/s41467-019-09234-6.
[27] R. Gaujoux, C. Seoighe, A flexible R package for nonnegative matrix factorization, BMC Bioinf. 11 (2010) 367, https://doi.org/10.1186/1471-2105-11-367.
[28] Y.K. Yang, C.R. Ogando, C. Wang See, T.Y. Chang, G.A. Barabino, Changes in phenotype and differentiation potential of human mesenchymal stem cells aging in vitro, Stem Cell Res. Ther. 9 (1) (2018) 131, https://doi.org/10.1186/s13287-018-0876-3.
[29] S. Zimmermann, M. Voss, S. Kaiser, U. Kapp, C.F. Waller, U.M. Martens, Lack of telomerase activity in human mesenchymal stem cells, Leukemia 17 (6) (2003) 1146–1149, https://doi.org/10.1038/sj.leu.2402962.
[30] E.M. Horwitz, K. Le Blanc, M. Dominici, I. Mueller, I. Slaper-Cortenbach, F.C. Marini, R.J. Deans, D.S. Krause, A. Keating, International Society for Cellular T, Clarification of the nomenclature for MSC: the international society for cellular therapy position statement, Cytotherapy 7 (5) (2005) 393–395, https://doi.org/10.1080/14653240500319234.
[31] Z. Wang, C. Chai, R. Wang, Y. Feng, L. Huang, Y. Zhang, X. Xiao, S. Yang, Y. Zhang, X. Zhang, Single-cell transcriptome atlas of human mesenchymal stem cells exploring cellular heterogeneity, Clin. Transl. Med. 11 (12) (2021) e650, https://doi.org/10.1002/ctm2.650.
[32] C. Zhang, L. Zhou, Z. Wang, W. Gao, W. Chen, H. Zhang, B. Jing, X. Zhu, L. Chen, C. Zheng, et al., Eradication of specific donor-dependent variations of mesenchymal stem cells in immunomodulation to enhance therapeutic values, Cell Death Dis. 12 (4) (2021) 357, https://doi.org/10.1038/s41419-021-03644-5.
[33] M.A. Travis, D. Sheppard, TGF-beta activation and function in immunity, Annu. Rev. Immunol. 32 (2014) 51–82, https://doi.org/10.1146/annurev-immunol-032713-120257.
[34] V. de Araujo Farias, A.B. Carrillo-Galvez, F. Martin, P. Anderson, TGF-beta and mesenchymal stromal cells in regenerative medicine, autoimmunity and cancer, Cytokine Growth Factor Rev. 43 (2018) 25–37, https://doi.org/10.1016/j.cytogfr.2018.06.002.
[35] C. Sun, L. Wang, H. Wang, T. Huang, W. Yao, J. Li, X. Zhang, Single-cell RNA-seq highlights heterogeneity in human primary Wharton's jelly mesenchymal stem/stromal cells cultured in vitro, Stem Cell Res. Ther. 11 (1) (2020) 149, https://doi.org/10.1186/s13287-020-01660-4.
[36] C. Trapnell, D. Cacchiarelli, J. Grimsby, P. Pokharel, S. Li, M. Morse, N.J. Lennon, K.J. Livak, T.S. Mikkelsen, J.L. Rinn, The dynamics and regulators of cell fate decisions are revealed by pseudotemporal ordering of single cells, Nat. Biotechnol. 32 (4) (2014) 381–386, https://doi.org/10.1038/nbt.2859.
[37] P. Chen, S. Tang, M. Li, D. Wang, C. Chen, Y. Qiu, Z. Fang, H. Zhang, H. Gao, H. Weng, et al., Single-cell and spatial transcriptomics decodes wharton's jelly-derived mesenchymal stem cells heterogeneity and a subpopulation with wound repair signatures, Adv. Sci. 10 (4) (2023) e2204786, https://doi.org/10.1002/advs.202204786.
[38] Y. Zhang, T. Na, K. Zhang, Y. Yang, H. Xu, L. Wei, L. Xu, X. Yan, W. Liu, G. Liu, et al., GMP-grade microcarrier and automated closed industrial scale cell production platform for culture of MSCs, J Tissue Eng Regen Med 16 (10) (2022) 934–944, https://doi.org/10.1002/term.3341.
[39] C. Millan, L. Prause, Q. Vallmajo-Martin, N. Hensky, D. Eberli, Extracellular vesicles from 3D engineered microtissues harbor disease-related cargo absent in EVs from 2D cultures, Adv. Healthcare Mater. 11 (5) (2022) e2002067, https://doi.org/10.1002/adhm.202002067.
[40] L. Sun, Y. Ji, B. Chi, T. Xiao, C. Li, X. Yan, X. Xiong, L. Mao, D. Cai, A. Zou, et al., A 3D culture system improves the yield of MSCs-derived extracellular vesicles and enhances their therapeutic efficacy for heart repair, Biomedicine & pharmacotherapy = Biomedecine & pharmacotherapie 161 (2023) 114557, https://doi.org/10.1016/j.biopha.2023.114557.
[41] P. Silva Couto, M.C. Rotondi, A. Bersenev, C.J. Hewitt, A.W. Nienow, F. Verter, Q.A. Rafiq, Expansion of human mesenchymal stem/stromal cells (hMSCs) in bioreactors using microcarriers: lessons learnt and what the future holds, Biotechnol. Adv. 45 (2020) 107636, https://doi.org/10.1016/j.biotechadv.2020.107636.
[42] J.R.K. Samal, V.K. Rangasami, S. Samanta, O.P. Varghese, O.P. Oommen, Discrepancies on the role of oxygen gradient and culture condition on mesenchymal stem cell fate, Adv. Healthcare Mater. 10 (6) (2021) e2002058, https://doi.org/10.1002/adhm.202002058.
[43] L.A. Costa, N. Eiro, M. Fraile, L.O. Gonzalez, J. Saa, P. Garcia-Portabella, B. Vega, J. Schneider, F.J. Vizoso, Functional heterogeneity of mesenchymal stem cells from natural niches to culture conditions: implications for further clinical uses, Cell. Mol. Life Sci. 78 (2) (2021) 447–467, https://doi.org/10.1007/s00018-020-03600-0.
[44] Y. Huang, Q. Li, K. Zhang, M. Hu, Y. Wang, L. Du, L. Lin, S. Li, L. Sorokin, G. Melino, et al., Single cell transcriptomic analysis of human mesenchymal stem cells reveals limited heterogeneity, Cell Death Dis. 10 (5) (2019) 368, https://doi.org/10.1038/s41419-019-1583-4.
[45] T. Zhou, Z. Yuan, J. Weng, D. Pei, X. Du, C. He, P. Lai, Challenges and advances in clinical applications of mesenchymal stromal cells, J. Hematol. Oncol. 14 (1) (2021) 24, https://doi.org/10.1186/s13045-021-01037-x.
[46] K. Janebodin, Y. Zeng, W. Buranaphatthana, N. Ieronimakis, M. Reyes, VEGFR2-dependent angiogenic capacity of pericyte-like dental pulp stem cells, J. Dent. Res. 92 (6) (2013) 524–531, https://doi.org/10.1177/0022034513485599.

[47] L. Li, P. Tang, Z. Zhou, Q. Wang, T. Xu, S. Zhao, Y. Huang, F. Kong, W. Liu, L. Cheng, et al., GIT1 regulates angiogenic factor secretion in bone marrow mesenchymal stem cells via NF-kappaB/Notch signalling to promote angiogenesis, Cell Prolif. 52 (6) (2019) e12689, https://doi.org/10.1111/cpr.12689.
[48] G.D. Yancopoulos, S. Davis, N.W. Gale, J.S. Rudge, S.J. Wiegand, J. Holash, Vascular-specific growth factors and blood vessel formation, Nature 407 (6801) (2000) 242–248, https://doi.org/10.1038/35025215.
[49] M. Hoffman, The tissue factor pathway and wound healing, Semin. Thromb. Hemost. 44 (2) (2018) 142–150, https://doi.org/10.1055/s-0037-1606181.
[50] M.F. Cordeiro, A. Mead, R.R. Ali, R.A. Alexander, S. Murray, C. Chen, C. York-Defalco, N.M. Dean, G.S. Schultz, P.T. Khaw, Novel antisense oligonucleotides targeting TGF-beta inhibit in vivo scarring and improve surgical outcome, Gene Ther. 10 (1) (2003) 59–71, https://doi.org/10.1038/sj.gt.3301865.
[51] B. Khan, S. Rangasamy, P.G. McGuire, T.R. Howdieshell, The role of monocyte subsets in myocutaneous revascularization, J. Surg. Res. 183 (2) (2013) 963–975, https://doi.org/10.1016/j.jss.2013.02.019.